Compact Microwave Filter Designs based on Cavity Resonators

by

Yuan Sun

A Thesis Submitted in Partial Fulfillment

of the Requirements for the Degree of

Master of Applied Science

In

The Faculty of Engineering and Applied Science

Electrical and Computer Engineering

University of Ontario Institute of Technology

April 2016

TABLE OF CONTENTS

Chapter Page

LIST OF FIGURES

LIST OF ABBREVIATIONS

DRF	Dielectric Resonator Filter
HCFM	Hybrid-Coupled Filter Module
ADS	Advanced Design System
HFSS	High Frequency Structural Simulator
EM	Electromagnetic
SIR	Stepped-Impedance Resonator
MUX	Multiplexer
RF	Radio Frequency
GSMs	Global Systems for Mobile Communications
PE	Parameter Extraction
SM	Space Mapping
PEC	Perfect Electric Conductor

ABSTRACT

Cavity resonators are widely used in microwave filters and multiplexers due to their high quality factor and high power handling capability. Compact designs of these filters are important for practical applications, as they are generally bulky. In this thesis, two types of compact microwave filter designs based on cavity resonators are developed.

Firstly, through the use of additional posts in irises of a dielectric resonator filter (DRF), a dual-band filter can be achieved. Metal posts, which can be realized using screws, are applied in the irises of dielectric resonator filters working as capacitive obstacles. These posts along with the irises and dielectric resonator enclosure, which work below cut-off, can form the resonators to function as an evanescent mode filter. With the existing dielectric resonator filter, a dual-band filter design can be achieved. Using a properly designed coaxial input/output structure, the two passbands can be tuned individually and then combined together. An example of the dual-band filter is designed and simulated to verify the design concept.

A new compact design of a hybrid-coupled filter module (HCFM) is also introduced in this thesis, for applications in communication satellites as a combiner. A conventional HCFM consists of two complete 3dB hybrid couplers and two identical passband filters in the middle. In this work, we use the inter-resonator couplings between two filters to replace one of the branches in a 3dB hybrid coupler used in HCFM to make the design more compact. Implementation of the new design is realized using waveguide filters, dielectric resonator filters and coaxial cavity filters. In all cases, the new structure preserves the

responses of a conventional design. The circuit model in ADS and the 3D structure in electromagnetic (EM) simulator HFSS are built to verify the concept. Moreover, by using tuning screws in both cavity resonators and waveguide T-junctions, we achieve the tunability of the HCFM.

ACKNOELEDGEMENTS

I would like to thank my supervisor Dr. Ying Wang for her help and support. During my two years' study and research in the master's program, Dr. Ying Wang has always been ready and patient to help. I have learned a lot of research skills from her. Also, I would like to express my gratitude to all my colleagues and friends for their kind support and company. In the end, I am grateful to my parents for their love and support.

Yuan Sun

Oshawa, Ontario

March 18, 2016

CHAPTER 1

Introduction

1.1 Overview

RF/microwave filters and multiplexers are widely used in wireless and satellite applications. Requirements like low cost, small size, high power handling capability and low insertion loss lead to demand of new designs of filters.

Resonators, which are capable of storing both electric and magnetic energy, are the basic components in filters. There are various forms and configurations of resonators. Different resonators have different advantages and limitations. They can be mainly divided into three categories. The first group is the lumped-element LC resonators. In one single LC resonator, the electric energy is stored in the capacitor while the magnetic energy is stored in the inductor. The resonant frequency is the frequency at which the electric energy equals to the magnetic energy. The second group is the planar resonators, which can take forms of microstrip transmission line, ring or patch resonators. Resonant frequency of a

planar resonators is determined by its physical dimensions together with the dielectric constant and height of its substrate. The third group is the cavity-type resonators, which include waveguide resonators, coaxial resonators and dielectric resonators.

Filters based on cavity resonators have the advantages of low insertion loss and high power handling capability compared to the other two types of filters. That's why they are widely used in the wireless and satellite applications. However, they are generally bulky, which makes the compact design of this type of filters important.

1.2 Multiple Bands Filters

Requirements like efficient use of frequency spectrum in satellite and wireless applications lead to emerging demand of multiple bands filters. Currently, there are several ways to implement a dual passband filter, including a cascade connection of a wide passband filter and a narrow stopband filter [1], and a combination of single filter and extra resonator sections [2]. Also, by using resonators containing open or short stubs, three transmission zeros can be achieved resulting in two passbands to create a dual-band filter [3]. Dual-band filters can also be realized by using stepped-impedance resonator (SIR) [4]. A method of combining stubs with SIR is also used in designing the dual-band filter [5]. Most of the multiple passbands filters focus on microstrip filters and other planar filters. In this thesis, we achieve dual-band filter by using a combination of dielectric resonator filter (DRF) and evanescent mode filter.

The concept of dielectric resonator filter was first introduced in 1960s. A single resonator in DRF contains the metal enclosure operating below cut-off, a dielectric puck and a support. A DRF takes the configuration of a number of dielectric resonators combined with coupling sections between resonators. Different methods have been developed to achieve the coupling between resonators in DRF including opening irises, coupling screws, coupling loops and notches in the wall.

In waveguide cavities, when frequency is below cutoff, we call it evanescent mode. Resonators may be formed by adding proper capacitance along the evanescent mode waveguide. These resonators can be employed to design evanescent mode filters.

1.3 RF combiners

In the last few decades, requirements like feeding several RF channels into one single antenna in a multiuser environment lead to the development of RF combiners. The combiner, also called output multiplexer (Output MUX), aims to combine different RF channels into one port. Different configurations of the combiners have been developed over the last forty years including circulator-coupled MUX, directional filter combiner, manifold multiplexer, and Hybrid-Coupled Filter Combiner Module (HCFM) multiplexer. The HCFM multiplexers have the advantage of no interaction between channel filters. Also, the power is equally divided into each filter, which increases the power handling capability. However, due to the need of two identical filters and also two hybrids for each channel, the weight and size are larger than other types of multiplexers.

1.4 Motivation

Dual-band/multiple-band filters are important components in wireless and satellite communication systems due to the requirement of efficient utilization of frequency spectrum. Conventional designs of dual-band filters using planar resonator filters have the disadvantage of high insertion loss and low power handling capability. Filters based on cavity resonators have the advantages of low insertion loss and high power handling capability. However, they are generally bulky, which makes the compact design of filters using cavity resonators important. In this thesis, a new approach of designing a dual-band filter is demonstrated by applying additional posts in the irises of a dielectric resonator filter (DRF) to form an extra evanescent mode filter.

The HCFM multiplexers are widely used as RF combiners in wireless and satellite communication systems. They have the advantages of no interaction between channel filters and high power handling capability. However, in conventional designs of a HCFM, two complete 3dB hybrids are used on each side of the passband filters in the middle, which makes the size large. In the new design of a HCFM, we use the inter-resonator couplings between two filters to replace one branch in a 3dB hybrid coupler to make the design of HCFM more compact.

1.5 Outline

In this thesis, we focus on cavity resonator filters and some advanced designs based on cavity resonator filters, including the multiple-band filters and HCFM in RF combiners.

In chapter 2, recent research advances have been reviewed on the multiple-band filter designs. Different methods to achieve dual passband filters have been studied. Also, we review the works on dielectric resonator filters and evanescent mode filters, based on which the new dual-band design is developed. Then we proceed to the development of multiplexers in communication and satellite systems. The works on HCFM designs and improvements are also studied.

In chapter 3, we focus on the design process of a new dual-band filter based on two kinds of cavity resonator filters, which are DRF and evanescent mode filter. A design example has been simulated in HFSS to verify the design concept.

In chapter 4, a new design of HCFM has been introduced. By using inter resonator coupling between two filters to replace one branch in a 3dB hybrid, the size becomes more compact. Different configurations have been implemented and simulated both in ADS and HFSS. Moreover, the center frequency can be tunable by adding screws in cavity resonators and waveguide sections in the new design of HCFM.

In chapter 5, we draw the conclusions from our new designs in chapter 3 and chapter 4. Also we present some future work in our research.

CHAPTER 2

Literature Review

Filters are one of the most important components in any RF/microwave communication systems. Cavity resonators are widely used in the designs of microwave filters where high Q value and high power handling capability are essential. Advances have been achieved in this area in the last few decades. In this chapter, we will review the previous works on cavity resonator filter designs and also some advanced designs based on cavity resonators, including dual passband filter and the HCFM implemented in RF combiners.

2.1 Cavity Resonator Filters

The filters based on cavity resonators have the advantages of low insertion loss and high power handling capability compared to the filters based on lumped-element LC resonators

or planar resonators. Cavity resonator filters are widely used in the wireless and satellite applications.

There are different technologies for implementing the cavity resonators, including rectangular/circular waveguide resonator, coaxial resonator, and dielectric resonator. Rectangular/circular waveguide resonators are rectangular/circular waveguides with both ends terminated in a short circuit. Similarly, a section of coaxial transmission line can be short circuited at both ends to form a coaxial resonator. Field distribution of different modes in these waveguides are well analyzed in the literature [6, 7].

The concept of dielectric resonator filter was first introduced in 1960s [8]. At that time, the dielectric resonator filters were not able to be used in applications due to the poor thermal stability of dielectric material. Advances in decreasing the temperature drift of dielectric material lead to the practical use of dielectric resonator filters. A single dielectric resonator contains the metal enclosure operating below cut-off, a dielectric puck and a support. It is difficult to calculate the resonant frequency, field distribution in dielectric resonators directly. Methods like mode matching technique [9, 10], finite-element analysis, and integral equation technique are applied for calculations. Electromagnetic (EM) simulation software, such as HFSS, can be used in calculating the resonant frequency and field distribution in dielectric resonator.

A dielectric resonator filter usually consists of a number of resonator cavities separated by irises to achieve inter resonator couplings. Different methods have been developed to achieve the coupling between resonators in DRF including opening irises, coupling screws, coupling loops, and notches in the wall.

There are various modes in dielectric resonators including TEH, TEE, TME, TMH, HEE and HEH. The single mode filter operating at $TE_{10\delta}$ mode is the most frequently used design in application. The dual-mode, triple-mode even quadruple-mode dielectric resonator filters also have been investigated. These designs have the advantage of volume saving compared to the single-mode DRF. However the dielectric resonator pucks have irregular shapes in these designs, which makes the cost higher and tuning of the filter more difficult.

Overall, dielectric resonator filters have the advantages of high power handling capability and low insertion loss. The main drawback of dielectric resonator filters is the spurious performance. An approach of mixing coaxial cavity resonators and dielectric resonators together [11] is used to improve the spurious performance. Also by using a cascade connection of coaxial cavity filter and dielectric resonator filter [12], we can also improve the spurious performance. This method however will increase the overall size of the filter and increase the insertion loss. Another approach of reshaping the resonator structure is proposed in [13] to improve the spurious performance.

Another type of cavity resonator filter is the evanescent mode filter. In 1956, Lebedev and Guttsait predicted that resonators can be built in waveguides below cutoff [14]. In 1958, Jaynes used the term "ghost mode" [15] to describe the phenomenon. In 1961, Edson demonstrated that these resonators based on waveguide below cutoff have high Q-factor and proposed their use in filters [16]. A design theory for filters employing evanescent mode resonators was proposed by Craven in 1971 [17] by comparing evanescent mode waveguide to the lumped circuit. In 1977, Synder introduced some slight corrections to Craven's work**.** In 1992, through the use of evanescent mode band-pass irises tuned to the

dielectric resonator filter, Synder successfully suppressed the dielectric resonator spurious modes [18].

2.2 Multiple Passbands Filters

Research of multiple passbands filters had been largely ignored in the past. Recently, requirements like efficient use of frequency spectrum in satellite applications lead to emerging demand of multiple-band filters. For instance, global systems for mobile communications (GSMs) require the devices to operate at both 900 and 1800MHz. Different ways have been used to implement a dual-passband filter. In 2004, a method of connecting a wide passband filter and a narrow stopband filter has been introduced in [1]. A combination of single filter and extra resonator sections is used to achieve multiple passbands filters in [2]. Also, by using resonators containing open or short stubs, three transmission zeros can be achieved resulting in two passbands to create a dual-band filter [3]. In [4], dual-band filters are realized using stepped-impedance resonator (SIR), with simple structure and tunable frequency. A method of combining stubs with SIR is also used in designing the dual-band filter [5]. Most of these designs focus on microstrip filters and other planar filters, which do not provide high quality performance compared to cavity resonator filters, such as waveguide filters or dielectric resonator filters, in terms of insertion loss and power handling capability.

Implementations of multiple passbands filters based on cavity resonator filters are more challenging. In 1990, Chen proposed a new design of tunable dielectric resonator filter

which also has the dual-band behavior [19]. However, no additional explanation and investigation were given in the paper. In 2009, Zhang proposed a novel dual-band dielectric resonator configuration by using two attached ring dielectric resonators in the shape of an "8" [20]. With different sizes of the two ring resonators, the attached structure can operate at two different frequencies. However, due to the irregular shape of the dielectric resonator, the tuning of the filter is difficult and also the cost of fabrication becomes high.

2.3 HCFM in RF Combiner (Output Multiplexer)

Requirements of separating or combining a number of RF channels lead to the development of multiplexers in communication and satellite systems. Multiplexers can be divided into two groups: channelizers and combiners. Channelizers are used to separate a wideband channel into several narrowband channels. Combiners are employed to combine a number of narrowband channels to connect to the antenna [21].

The concept of separating or combining signals at different frequencies to connect with one single antenna was proposed for many years. However it was not until the advent of satellite communication systems that advances were achieved in the design of multiplexers.

Different configurations of the multiplexers have been developed over the last few decades (since 1970s) including circulator-coupled MUX, directional filter MUX, manifold MUX and hybrid-coupled MUX [22-28]. Circulator-coupled multiplexers can only handle a low power level. Directional filter multiplexers have the limitations of small bandwidth and they are rarely implemented in high-power combining systems. In practical

applications of combiners, the manifold coupled multiplexer and hybrid coupled multiplexers are most frequently used [29-30].

A HCFM is a building block of a HCFM multiplexer. A conventional HCFM consists of two 3dB hybrids and two identical bandpass filters as shown in Fig. 2.1 [29].

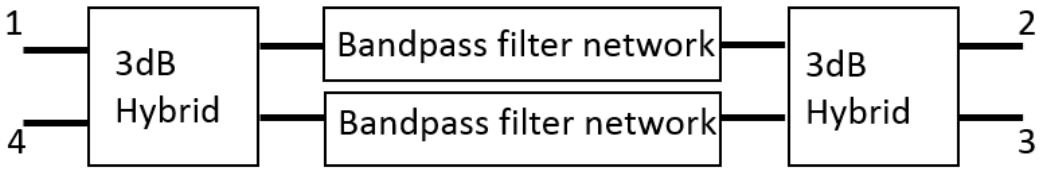

Figure 2.1. Hybrid-coupled filter module (HCFM) [29].

With inputs at port 1 and the port 2 terminated, the out-of-band channels will emerge from port 4 and the in-band channel will emerge at port 3 of the HCFM, when used as channelizers.

A number of HCFMs can be connected together as shown in Fig 2.2 [29] to form a combiner. In Fig. 2.2, four different channels are input at four different HCFMs. According to the properties of a HCFM, the in-band channel at each module and the channels come from previous HCFMs will all emerge at the same port. In the end, the four different channels will be combined and emerge at the common output.

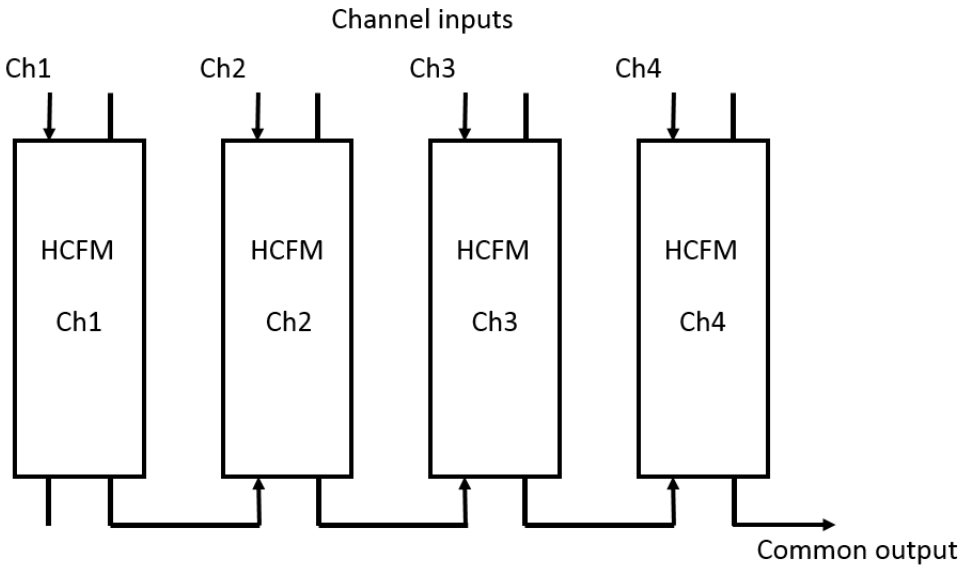

Figure 2.2. Combiner with HCFMs [29].

A 3dB hybrid is also called the quadrature hybrid. It is a 4-port network as shown in Fig. 2.3 [7]. With power entered in port 1, it is equally divided between port 2 and port 3, the port 4 is isolated. There is a -90° phase shift from port 1 to port 2, and there is a -180° phase shift from port 1 to port 3.

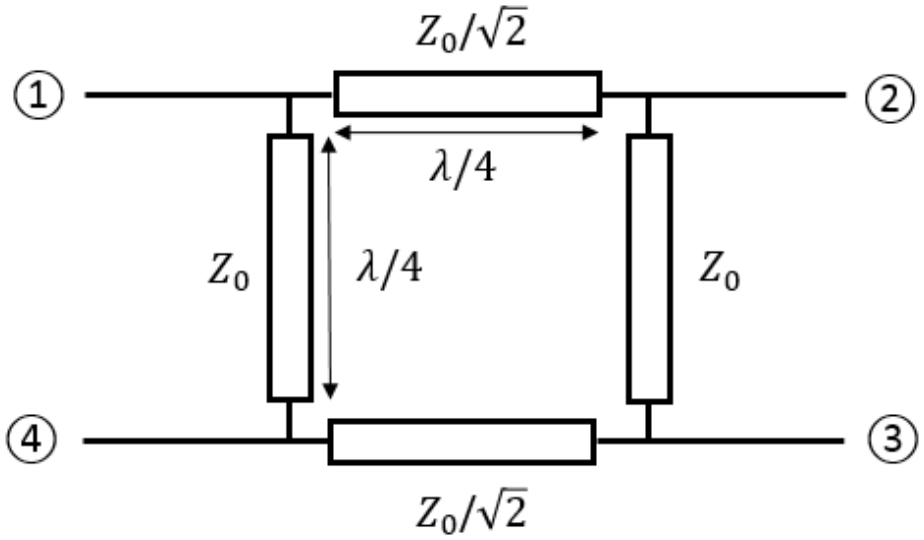

Figure 2.3. A 3dB hybrid coupler [7].

The S matrix of a 3 dB hybrid coupler has the following form:

$$[s] = \begin{bmatrix} 0 & j & 1 & 0 \\ j & 0 & 0 & 1 \\ 1 & 0 & 0 & j \\ 0 & 1 & j & 0 \end{bmatrix} \tag{2.1}$$

The 3 dB hybrid coupler can be made in the forms of microstrip lines. We can also use E-plane or H-plane waveguides, or coaxial transmission lines to build the coupler for high power applications.

In HCFM, the two identical bandpass filters can be cavity resonator filters, including waveguide filter, coaxial cavity filter and dielectric resonator filter.

In 2007, Rhodes proposed a new design method of the combiner by using two 3dB hybrids and two single resonators between them as one section [31]. A cascade connection of a number of these sections can achieve the function of a RF combiner. The main idea of this method is that each section corresponds to one pole in the desired filter transfer function. This makes the tunability of the combiner easier to be realized than conventional designs. In 2013, Hunter built a 4^{th} order combiner based on this method [32]. However, the drawback of this design is that in each section, there are two complete hybrid coupler, which makes the total size of the combiner extremely large. Moreover, no implementation in waveguide transmission lines has been reported.

2.4 Research Contribution

In this thesis, two compact microwave designs based on cavity resonators have been achieved.

In the design of a dual-passband filter, metal posts, which can be realized using screws, are applied in the irises between resonators in DRF [33]. The irises and the DRF resonator enclosures all work below cut-off. By adding these posts, which function as capacitive obstacles, along the metal enclosure, resonators can be formed to function as an evanescent mode filter. With proper positioning of the posts and right input/output coupling, an extra passband of evanescent mode filter can be achieved without any increase in size. The electromagnetic fields of the two filters are mainly orthogonal to each other. A dual-band filter is designed. Simulation result shows good verification of the concept.

In the design of a new HCFM used in multiplexer, we use the inter-resonator couplings between two filters to replace one branch in a 3dB hybrid coupler to make the design more compact. The 3 dB hybrid can be replaced by two H-plane/E-plane waveguide T-junctions or two coaxial transmission line T-junctions. The two identical filters in HCFM can take forms of different cavity resonator filters including rectangular waveguide filter, coaxial cavity filter, and dielectric resonator filter. The new design preserves the function of a conventional HCFM design with a much more compact structure. Moreover, through the use of tuning screws in both cavity resonators and waveguide T-junctions, we achieve the tunability of the HCFM.

CHAPTER 3

Design of Dual-Band Filter

3.1 Dielectric Resonator Filter

The design process of a filter usually consists of a number of steps [34-35]. First, according to the specific requirements, such as center frequency, bandwidth and return loss, the filter order and function need to be determined. In the second step, we need to synthesize the circuit model of the desired filter function. For example, the coupling matrix model [36-37] is a widely used circuit model. After the synthesis of the circuit model, the type of filter needs to be determined based on the size, insertion loss and power handling capability requirements. The last step then is to identify the physical dimensions of the filter.

The structure of a conventional three pole DRF is shown in Fig. 3.1. It contains three dielectric resonators operating at $TE_{01\delta}$ mode. The inter-resonator coupling is achieved by irises. The input/output coupling is realized using probes. For the design process of DRF, we use the coupling matrix circuit model together with the electromagnetic (EM) solver, HFSS, to synthesize the physical dimensions.

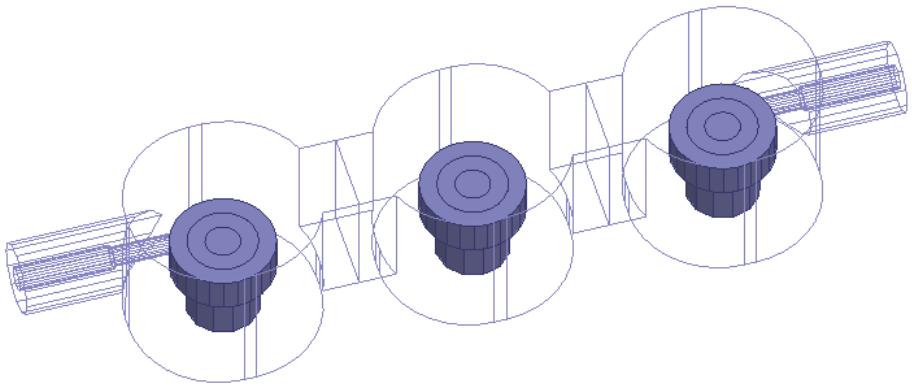

Figure 3.1. Perspective view of the DRF.

For required center frequency, one single dielectric resonator is simulated in HFSS [29], as shown in Fig. 3.2, to get the dimensions of enclosure cavity, support, and the dielectric puck. During the tuning process of center frequency in HFSS, we keep the radius of the dielectric pucks a constant, and the resonant frequency of the resonator is determined by the height of the puck.

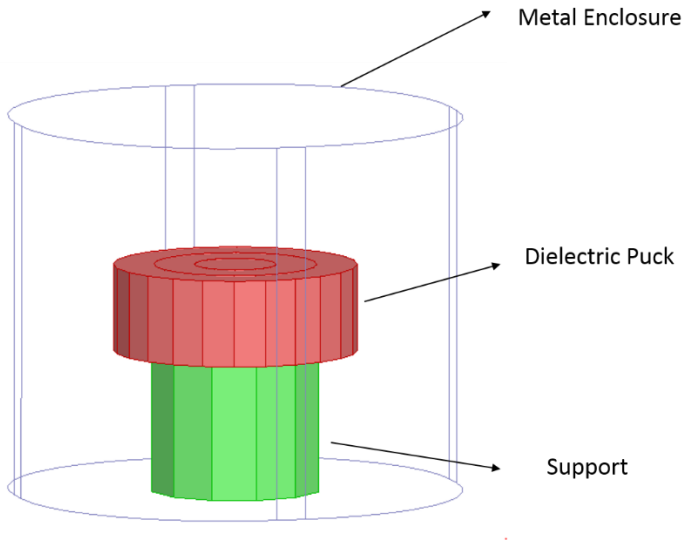

Figure 3.2. One single dielectric resonator [29].

Two-coupled resonator structure built in HFSS, as shown in Fig. 3.3, is used in the calculation of coupling between resonators. The two resonators in Fig 3.3 have the same dimensions. By changing the size of the iris between the two resonators, the coupling value can be changed. In circuit model, symmetry is used to divide the coupling between two adjacent resonators into single resonators terminated by a magnetic wall (even mode) and an electric wall (odd mode). The frequencies f_m and f_e are the resonant frequencies of the two circuits [29]. Inter-resonator coupling M_{ij} can be calculated from the two resonant frequencies f_m and f_e as in (3.1).

$$M_{ij} = \frac{({f_e}^2 - {f_m}^2)}{({f_e}^2 + {f_m}^2)} \times \frac{f_0}{BW} \tag{3.1}$$

In HFSS, we can get the two resonant frequencies f_m and f_e directly by performing eigen mode simulations.

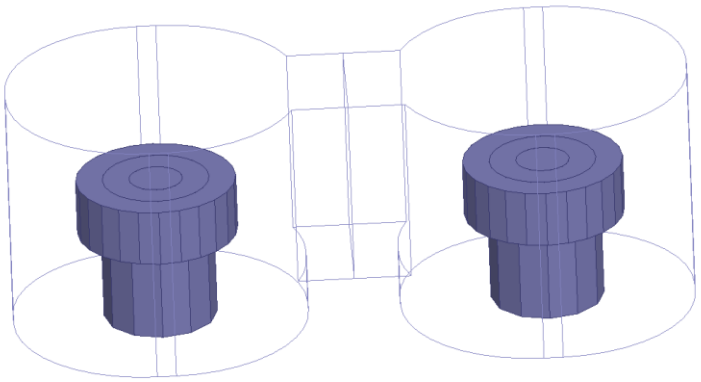

Figure3.3. Two-coupled resonator structure for coupling calculation.

The input and output couplings are calculated from the group delay obtained using HFSS. The structure used in HFSS is shown in Fig. 3.4. Only one probe is built in the structure. The input/output coupling value can be changed by changing the position and depth of the probe. The relationship between group delay τ and input/output coupling R is shown in (3.2) [29], where BW is the filter bandwidth.

$$R = \frac{2}{\pi \times BW} \times \frac{1}{\tau} \tag{3.2}$$

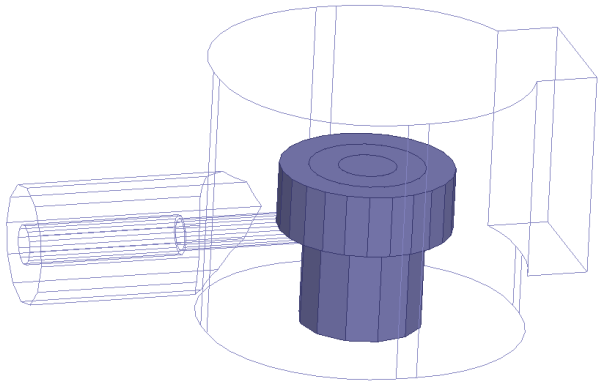

Figure 3.4. One probe structure for group delay simulation in HFSS.

By following the steps described above, we can get reasonable design dimensions. However, these values are not accurate once all resonators and I/O coupling structures are put together. The accuracy of this method is limited because of the interactions between components, and because elements in the circuit model are assumed to be frequency-independent. Therefore, the physical dimensions obtained thus far are considered as an initial design. Once the initial values for the dimensions of DRF are obtained, we need to fine tune the physical dimensions of the filter.

The optimization process [38-42] is shown in Fig. 3.5. In the process, the physical dimensions of the filter are iteratively modified until requirements are satisfied.

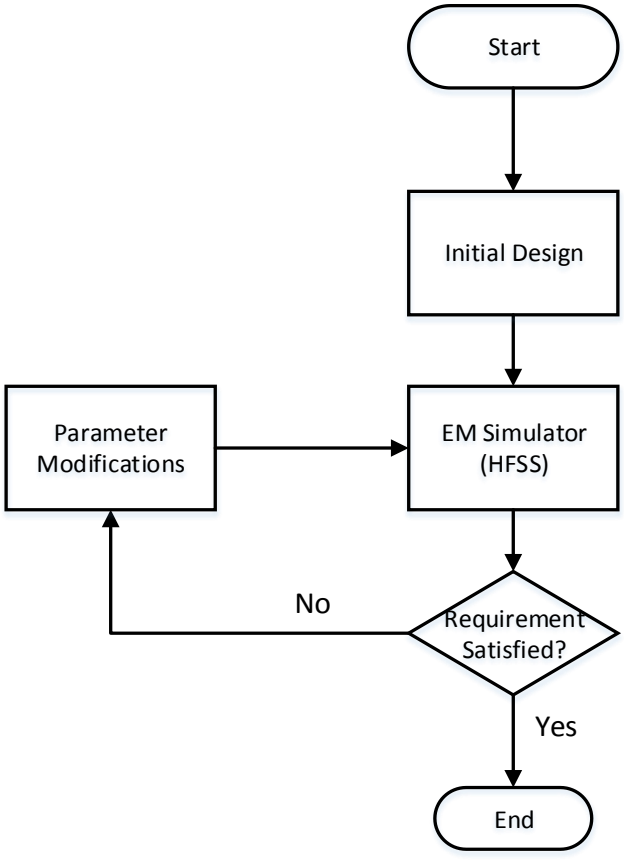

Figure 3.5. The optimization process.

In order to reduce the CPU time of the design process, parameter extraction (PE) in Space Mapping (SM) technique [43-51] is used to guide the fine tuning of the filter dimensions. The EM simulator, HFSS, which is accurate but time-consuming, is used as a fine model and the circuit model in ADS [52], which is fast but less accurate, serves as a coarse model. The main idea of SM method is to make use of the speed of the coarse model and the accuracy of the fine model.

Firstly, according to the original design specifications, we built the circuit model with optimized parameters in ADS. The initial design is simulated in HFSS, and the filter responses are used to exact circuit model parameters. By comparing the extracted circuit model parameters with those of the optimal circuit model, we can get an idea of how to modify the design parameters in HFSS. Then the fine model in HFSS is simulated with the modified parameters. After that, PE is performed on the new results from HFSS and compared to the optimal coarse model parameters. After several iterations, the responses from HFSS meet the design specifications, and we can achieve the final dimensions of the 3-pole dielectric resonator filter.

The structure in Fig. 3.1 is built using the process as above. The electric field distribution in the cavity is shown in Fig. 3.6.

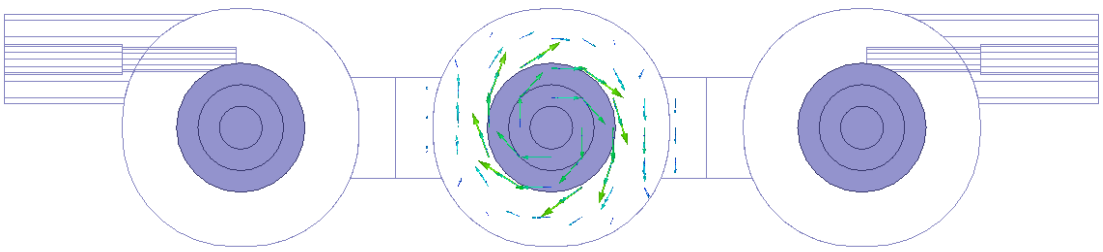

Figure 3.6. The electric field distribution in DRF.

3.2 Evanescent Mode Filter Design

The design of an evanescent mode filter follows the same process as for the DRF. A realization of the filter using the DRF housing is shown in Fig. 3.7. The dielectric resonator enclosures along with the rectangular waveguide irises work below cutoff (evanescent mode).

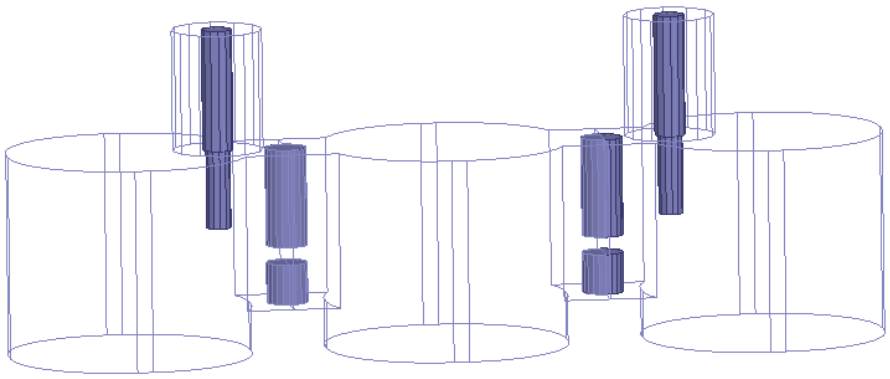

Figure 3.7. Perspective view of the evanescent mode filter.

The center frequency is mainly determined by the gap between the vertical posts in each iris of the DRF. The inter-resonator coupling is related to the distance between two posts in different irises. The longer the distance is, the smaller the coupling. The depth of the probe in the cavity and also the distance between the probe and the post determine the input/output coupling.

In a conventional design of a coaxial cavity filter [53-58], the gap is usually between one end of the vertical post and the housing. Designs with this structure are easier to

fabricate. However, in this case, the location of the gap is chosen to be closer to the middle of the iris because the fields of the DRF are stronger in the middle area. These posts will have less effect on the DRF when the gaps are closer to the middle.

Moreover, the electric field of the evanescent mode filter is oriented vertically in the gap between the vertical posts as shown in Fig. 3.8.

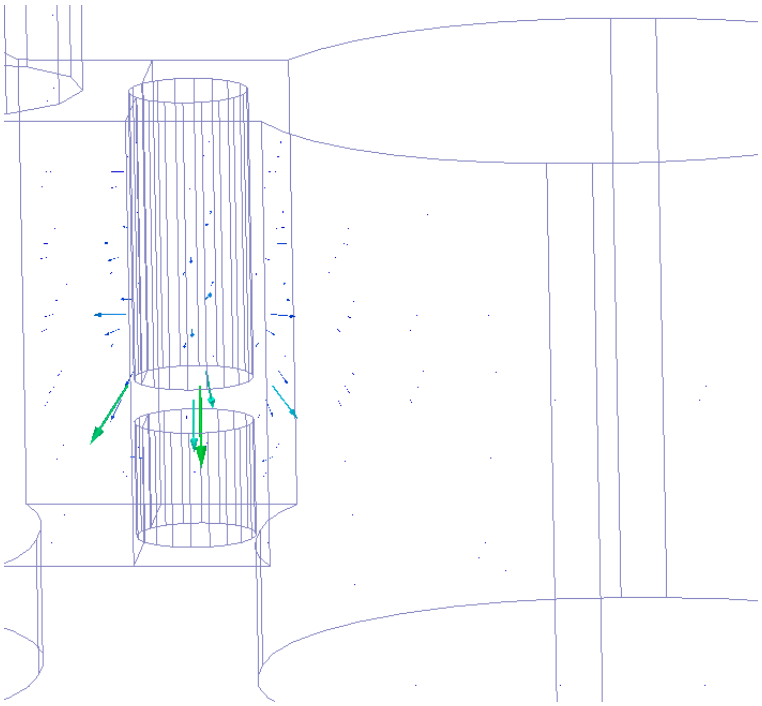

Figure 3.8. The electric field distribution between vertical posts.

3.3 Input/Output Probe Design for Dual-Band Filter

As discussed above, the EM fields of the two filters are mainly orthogonal to each other. By applying proper input/output coupling for two filters, a dual-band filter can be achieved. A new structure of the input/output coaxial probe is used in this thesis as shown in Fig. 3.9.

The probe has a vertical section and also a horizontal section to provide couplings for both filters.

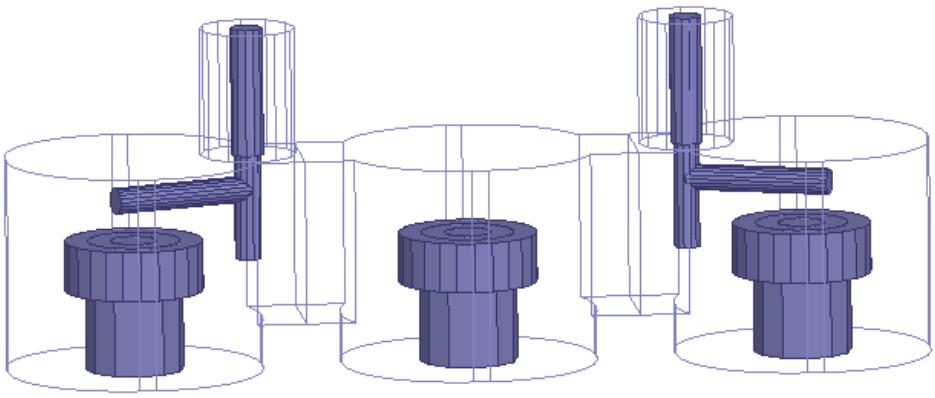

(a)

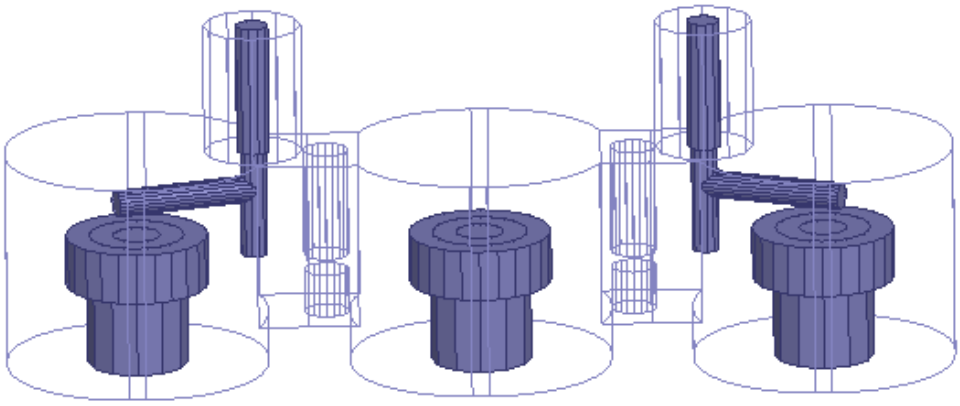

(b)

Figure 3.9. Perspective view of input/output structure in (a) the dielectric resonator filter, and (b) the evanescent mode filter with the DRF detuned.

The vertical section of the probe mainly provides the input/output coupling for the evanescent mode filter while the horizontal section provides the coupling for the DRF.

With the structures shown in Fig. 3.9(a) and Fig. 3.9(b), the two filters can be tuned individually and then combined together. For the structure in Fig. 3.9(a), the input/output coupling can be tuned by changing the height and length of the horizontal section of the probe structure. The direction of the section can also be changed in order to realize the required coupling. For the structure in Fig. 3.9(b), the dielectric pucks are detuned to evaluate the response of only the evanescent mode filter. We set the material of the dielectric pucks as perfect electric conductor (PEC) to move the center frequency of DRF away from the center frequency of the evanescent mode filter. In this way, we can evaluate the response of only the evanescent mode filter. The input/output coupling can be tuned by changing the position of the probe and by changing the depth of the vertical section.

The S parameters of two single filters in Fig. 3.9 are shown in Fig. 3.10. For the dielectric resonator filter alone, the center frequency is at 12.8GHz and the bandwidth is about 50MHZ. For the evanescent mode filter alone, the center frequency is at 12.47GHz and the band width is around 75MHz.

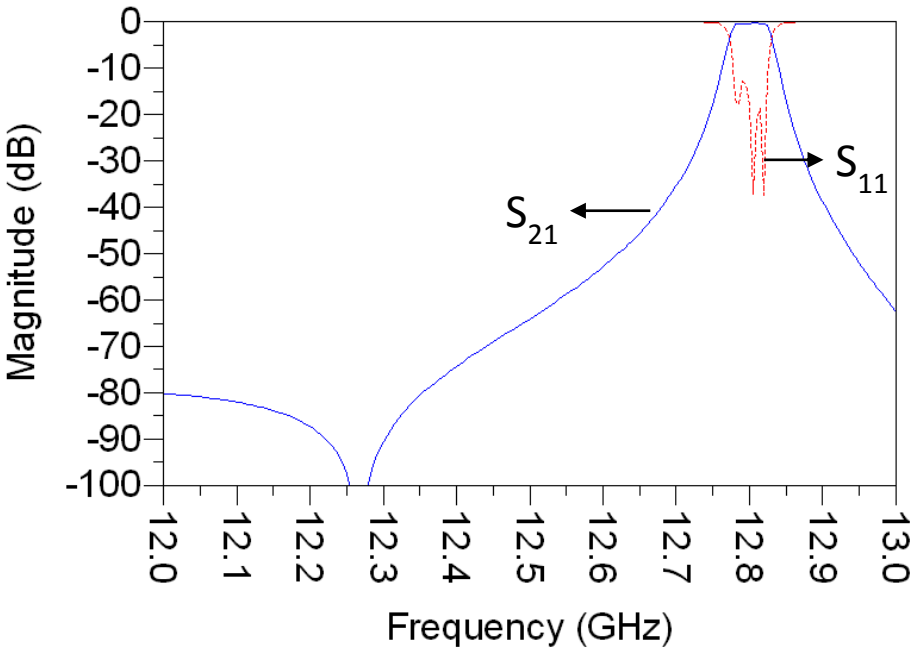

(a)

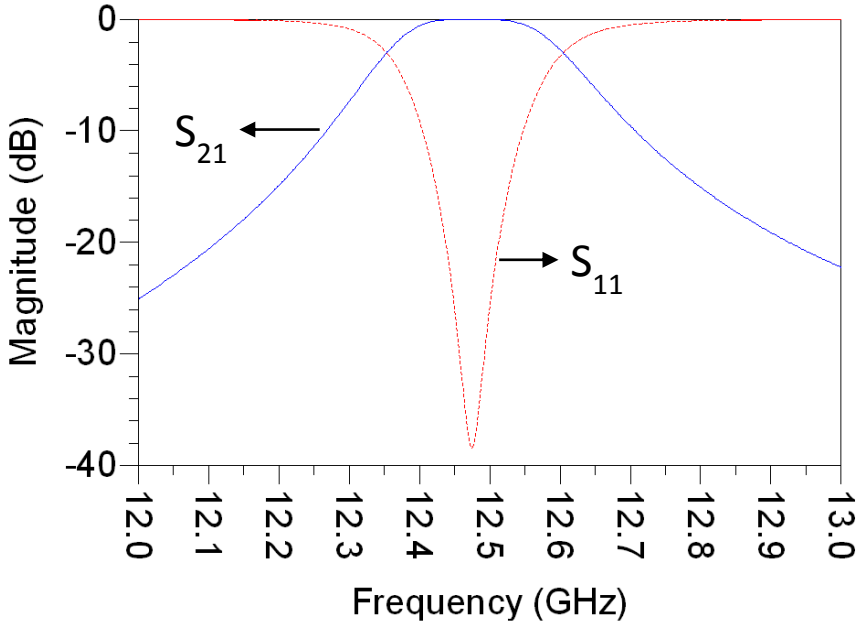

(b)

Figure 3.10. S_{11} and S_{21} of (a) the dielectric resonator filter, and (b) the evanescent mode filter.

3.4 Design Example

An example of this dual-band filter is simulated in order to verify the design concept. As shown in Fig. 3.11, a three pole dielectric resonator filter operating at 12.8GHz and an evanescent mode filter operating at 12.47GHz are combined together, which makes the size of the filter extremely compact. The EM responses from HFSS are shown in Fig. 3.12.

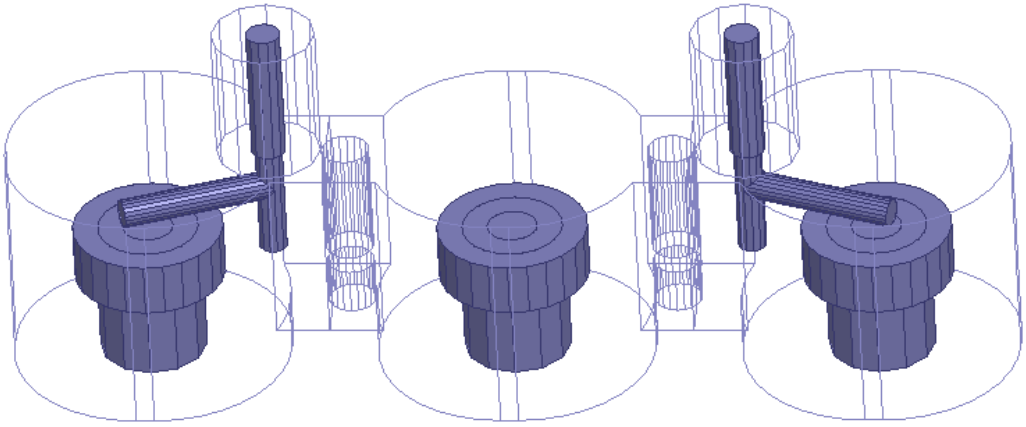

Figure 3.11. Perspective view of the dual-band filter.

By comparing Fig. 3.10 and Fig. 3.12, we can see when the two filters are combined together, there is a small shift of the center frequency for each filter. The center frequency of the evanescent mode filter changes from 12.47GHz to 12.42GHz, and the center frequency of DRF changes from 12.8GHZ to 12.82GHz. This is due to the interaction between the two filters.

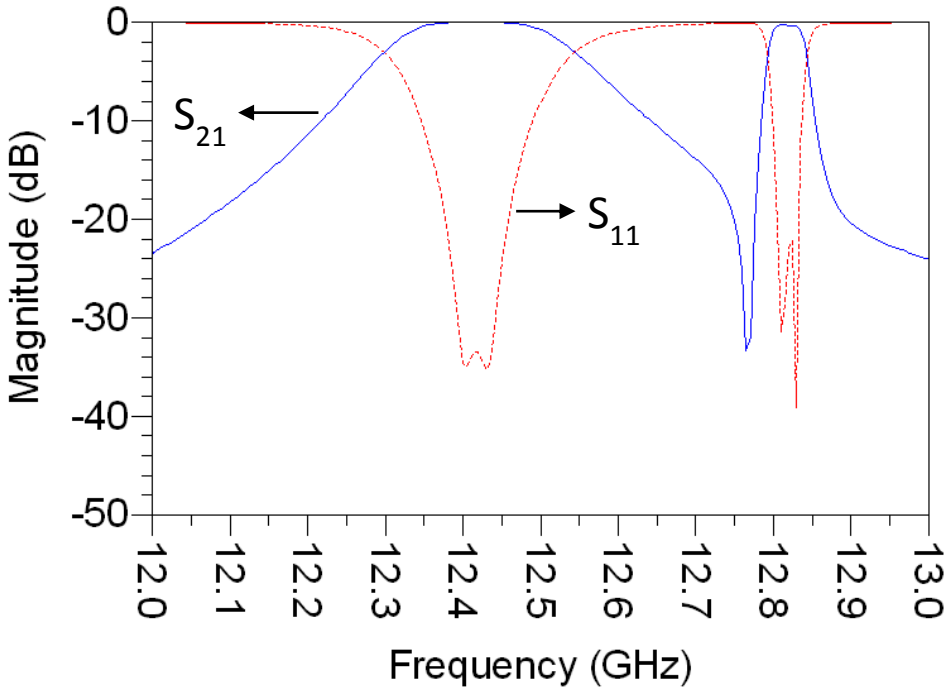

Figure 3.12. S_{11} and S_{21} of the dual-band filter.

3.5 Summary

In chapter 3, we first explained the design process of two types of filters, namely the dielectric resonator filter and the evanescent mode filter. Then, through the use of additional posts in irises of a dielectric resonator filter (DRF), a dual-band filter is achieved. Metal posts, which are realized using screws, are applied in the irises of the dielectric resonator filter working as capacitive obstacles. These posts along with the irises and dielectric resonator enclosures, which work below cut-off, form the resonators to function as an evanescent mode filter. With the existing dielectric resonator filter, a dual-band filter design is achieved. An example of this dual-band filter is simulated. The three pole

dielectric resonator filter operating at 12.8GHz and the evanescent mode filter operating at 12.47GHz are combined together.

CHAPTER 4

Design of HCFM

4.1 Development of the New HCFM

A basic 4-port device used in combiners is shown in Fig. 2.1 known as a hybrid-coupled filter module (HCFM). With inputs at port 1 and the port 2 terminated with matched load, the out-of-band channels will emerge from port 4 and the in-band channel will emerge at port 3.

In each HCFM of the combiner in Fig. 2.2, there are two identical bandpass filters and two 3dB hybrid couplers. A branch-line 3dB hybrid coupler and its normalized form [7] are shown in Fig. 4.1.

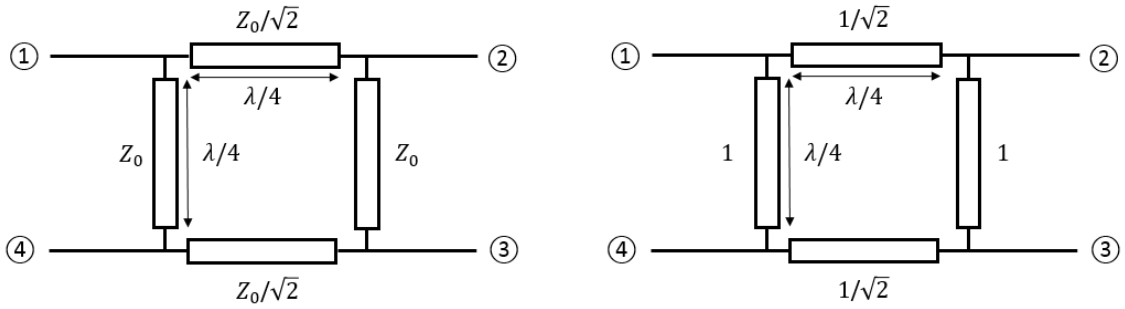

Figure 4.1. A 3dB branch-line coupler and its normalized form [7].

In this thesis, we use the inter-resonator couplings between two filters to replace one of the branches in a 3dB hybrid coupler to make the design more compact. The two structures are compared in Fig. 4.2 and Fig. 4.3, in which the passband filters are two identical 3-pole waveguide filters.

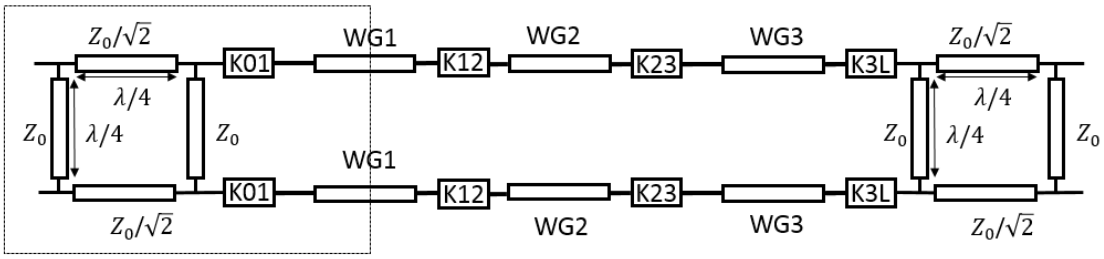

Figure 4.2. Circuit model of a conventional HCFM.

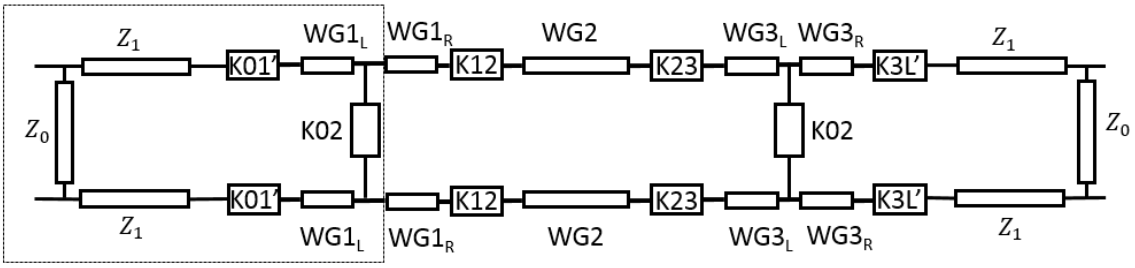

Figure 4.3. Circuit model of the new design of HCFM.

In Fig. 4.3, K_{02} is the coupling between two filters, and there are two of them in the new design of HCFM. The first and the last waveguide resonators are divided into two parts by the K_{02} coupling section. K_{01}' and K_{3L}' are the input and output couplings in the new design of HCFM.

The even-odd mode decomposition technique is used to analyze the two HCFMs [59].

First, we discuss the even-odd mode decomposition technique used in the analysis of a 3dB hybrid coupler. The decomposition of a 3dB branch-line coupler is shown in Fig. 4.4 [7].

The excitation entered at port 1 can be decomposed into the superposition of an even-mode excitation and an odd-mode excitation. The sum of the responses to the two excitations is the actual response to the original excitation, which is incident at port 1. We set the amplitude of wave entered at port 1 as 1. As shown in Fig. 4.4, in each mode, due to the symmetry or anti-symmetry of the excitation, the four-port network can be decomposed into two decoupled two-port networks. In even-mode, the two excitations are both +1/2. In odd-mode, the two excitations are +1/2 and -1/2, respectively. After this, each two-port network can be easily characterized using its *ABCD* matrix. The *ABCD* matrix of the two-port network can be calculated by multiplying the *ABCD* matrices of each cascade component. The *ABCD* matrices of some useful circuits are shown in Fig. 4.5 [59].

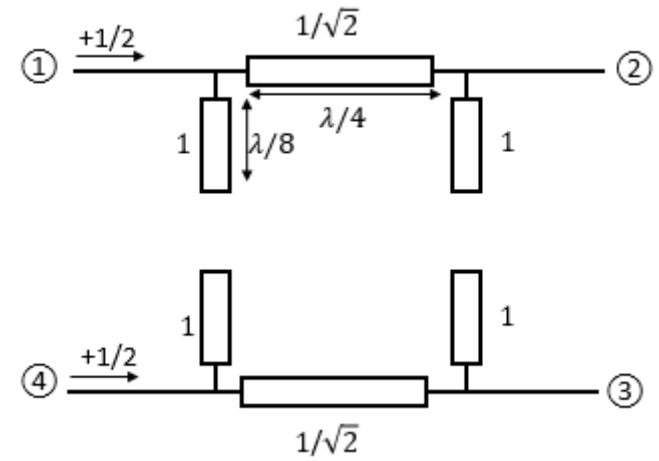

(a)

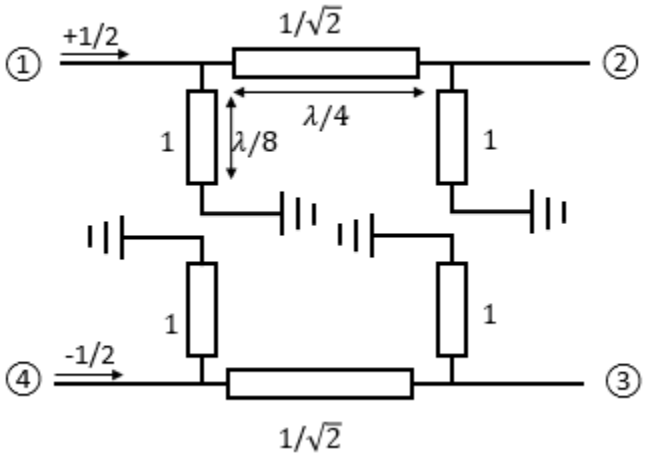

(b)

Figure 4.4. Decomposition of the 3dB coupler into (a) even-mode exciton, and (b) odd-mode excitation [7].

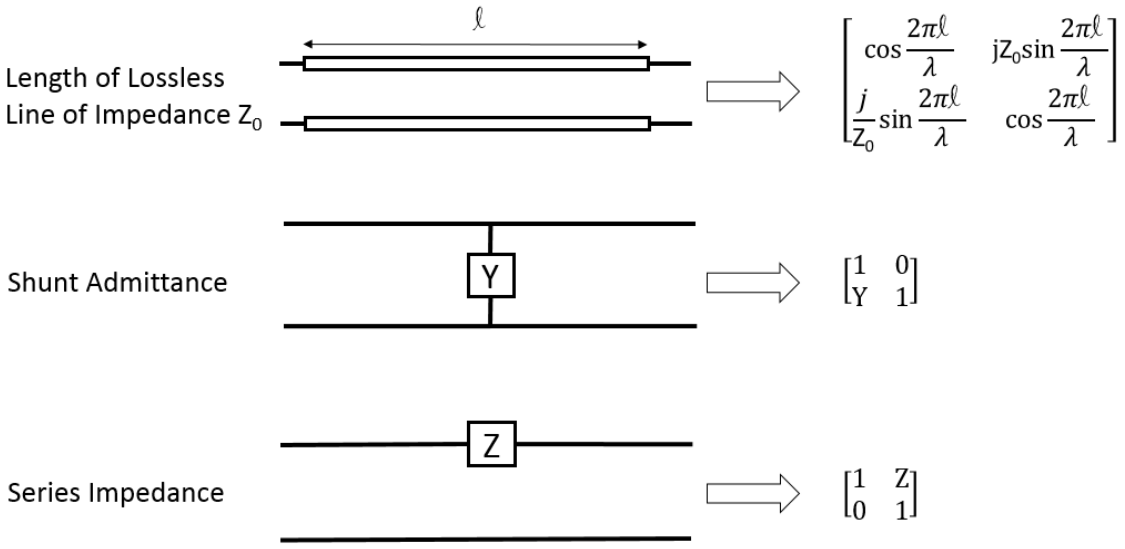

Figure 4.5. The *ABCD* matrices for some useful circuits [59].

For example, the *ABCD* matrix of the even-mode two-port network for the branch-line coupler is shown in (4.1).

$$\begin{bmatrix} A & B \\ C & D \end{bmatrix} = \begin{bmatrix} 1 & 0 \\ j & 1 \end{bmatrix} \begin{bmatrix} 0 & \frac{j}{\sqrt{2}} \\ j\sqrt{2} & 0 \end{bmatrix} \begin{bmatrix} 1 & 0 \\ j & 1 \end{bmatrix} \tag{4.1}$$

In (4.1), $\begin{bmatrix} 1 & 0 \\ j & 1 \end{bmatrix}$ is the *ABCD* matrix for the shunt open-circuited $\boldsymbol{\lambda}/8$ stub. The admittance of the shunt stub *is* $Y = j\tan\beta l = j$. Therefore according to Fig. 4.5, the *ABCD* matrix is $\begin{bmatrix} 1 & 0 \\ j & 1 \end{bmatrix}$. Similarly, $\begin{bmatrix} 0 & j/\sqrt{2} \\ j\sqrt{2} & 0 \end{bmatrix}$ is the *ABCD* matrix for the $\boldsymbol{\lambda}/4$ transmission line with the $1/\sqrt{2}$ characteristic impedance because $\sin\frac{2\pi l}{\lambda} = 1$ and $\cos\frac{2\pi l}{\lambda} = 0$.

The two structures in Fig. 4.2 and Fig. 4.3 can also be analyzed using the even and odd mode excitations. For the two structures in Fig. 4.2 and Fig. 4.3, the *ABCD* matrix should

be the same for both even mode and odd mode if we want the new design of HCFM to have the same function as a conventional design.

Due to the symmetry and similarity of the structure, we only need to compare the *ABCD* matrices of the two structures in the dashed-line boxes in Fig. 4.2 and Fig. 4.3, as shown in Fig. 4.6.

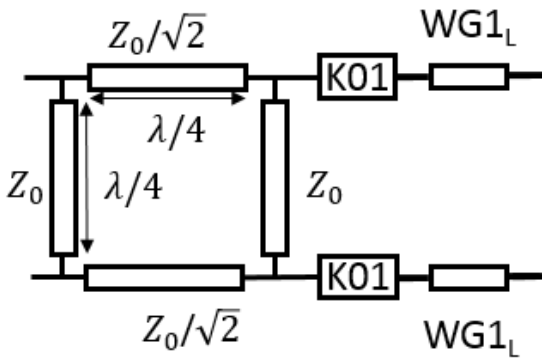

(a)

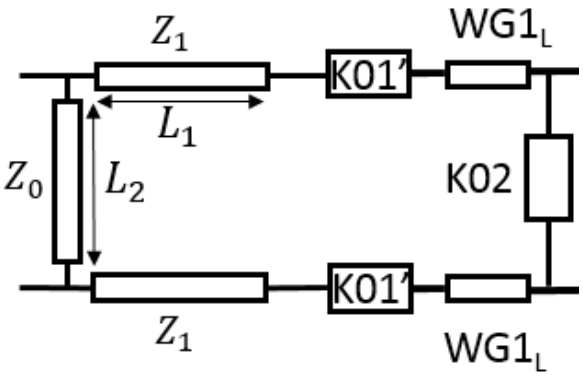

(b)

Figure 4.6. Structure in the dashed-line box in (a) Fig. 4.2, and (b) Fig. 4.3.

The *ABCD* matrix of a conventional HCFM shown in Fig. 4.6(a) in even mode is shown in (4.2).

$$\begin{bmatrix} A & B \\ C & D \end{bmatrix} = \begin{bmatrix} 1 & 0 \\ j & 1 \end{bmatrix} \begin{bmatrix} 0 & \frac{j}{\sqrt{2}} \\ j\sqrt{2} & 0 \end{bmatrix} \begin{bmatrix} 1 & 0 \\ j & 1 \end{bmatrix} \begin{bmatrix} 0 & jK_{01} \\ \frac{j}{K_{01}} & 0 \end{bmatrix} \begin{bmatrix} 0 & j \\ j & 0 \end{bmatrix} = \begin{bmatrix} \frac{K_{01}}{\sqrt{2}} & \frac{-j}{\sqrt{2}K_{01}} \\ -\sqrt{2}jK_{01} & 0 \end{bmatrix} \quad (4.2)$$

where $\begin{bmatrix} 0 & jK_{01} \\ j/K_{01} & 0 \end{bmatrix}$ is the *ABCD* matrix for the input coupling, and $\begin{bmatrix} 0 & j \\ j & 0 \end{bmatrix}$ is the *ABCD* matrix for the $\boldsymbol{\lambda}/4$ waveguide with the impedance Z_0=1.

The *ABCD* matrix of the new design of HCFM shown in Fig. 4.6(b) in even mode is shown in (4.3).

$$\begin{bmatrix} A & B \\ C & D \end{bmatrix} = \begin{bmatrix} 1 & 0 \\ j & 1 \end{bmatrix} \begin{bmatrix} 0 & jZ_1 \\ \frac{j}{Z_1} & 0 \end{bmatrix} \begin{bmatrix} 0 & jK'_{01} \\ \frac{j}{K'_{01}} & 0 \end{bmatrix} \begin{bmatrix} 0 & j \\ j & 0 \end{bmatrix} \begin{bmatrix} 1 & 0 \\ jK_{02} & 1 \end{bmatrix} = \begin{bmatrix} \frac{Z_1K_{02}}{K'_{01}} & \frac{-jZ_1}{K'_{01}} \\ \frac{-jK'_{01}}{Z_1} & 0 \end{bmatrix} \quad (4.3)$$

where $\begin{bmatrix} 0 & jZ_1 \\ j/Z_1 & 0 \end{bmatrix}$ is the *ABCD* matrix for the L_1=$\boldsymbol{\lambda}/4$ transmission line with the characteristic impedance Z_1, $\begin{bmatrix} 0 & jK'_{01} \\ j/K'_{01} & 0 \end{bmatrix}$ is the *ABCD* matrix for the input coupling in the new HCFM, and $\begin{bmatrix} 1 & 0 \\ jK_{02} & 1 \end{bmatrix}$ is the *ABCD* matrix for the coupling section between two bandpass filters in even mode. The K_{02} section can be seen as a L_2=$\boldsymbol{\lambda}/4$ long transmission line with characteristic impedance K_{02}. In the even mode, the transmission line is open-circuited in the middle and the admittance of $\boldsymbol{\lambda}/8$ open-circuited stub is $Y = jZ\tan\beta l = jK_{02} * 1 = jK_{02}$. According to Fig. 4.5, the *ABCD* matrix is $\begin{bmatrix} 1 & 0 \\ jK_{02} & 1 \end{bmatrix}$.

For the *ABCD* matrices in (4.2) and (4.3) to be the same,

$$K'_{01} = \sqrt{2} * Z_1 * K_{01} \tag{4.4}$$

$$K_{02} = {K_{01}}^2 \tag{4.5}$$

where Z_0 is normalized to be 1, K_{01} is the filter input coupling in the conventional structure, K'_{01} is the filter input coupling in new structure, and K_{02} is the inter-resonator coupling between two filters. Z_1 is the characteristic impedance of the branch between port 1 and 2 of coupler in the new structure.

As shown in (4.4) and (4.5), if Z_1 is also set as 1, we need to enlarge the input coupling by $\sqrt{2}$. In addition, the coupling K_{02} equals to ${K_{01}}^2$.

We also apply these values to the *ABCD* matrices of the two structures under odd mode excitations. The *ABCD* matrix of a conventional HCFM shown in Fig. 4.6(a) in odd mode is shown in (4.6).

$$\begin{bmatrix} A & B \\ C & D \end{bmatrix} = \begin{bmatrix} 1 & 0 \\ -j & 1 \end{bmatrix} \begin{bmatrix} 0 & \frac{j}{\sqrt{2}} \\ j\sqrt{2} & 0 \end{bmatrix} \begin{bmatrix} 1 & 0 \\ -j & 1 \end{bmatrix} \begin{bmatrix} 0 & jK_{01} \\ \frac{j}{K_{01}} & 0 \end{bmatrix} \begin{bmatrix} 0 & j \\ j & 0 \end{bmatrix} = \begin{bmatrix} \frac{-K_{01}}{\sqrt{2}} & \frac{-\mathrm{j}}{\sqrt{2}K_{01}} \\ \frac{-jK_{01}}{\sqrt{2}} & \frac{-1}{\sqrt{2}K_{01}} \end{bmatrix} \tag{4.6}$$

In (4.6), $\begin{bmatrix} 1 & 0 \\ -j & 1 \end{bmatrix}$ is the *ABCD* matrix for the shunt short-circuited $\boldsymbol{\lambda}/8$ stub, the admittance of the shunt stub is $\mathrm{Y} = -\mathrm{j}\tan\beta l = -j$. According to Fig. 4.5, the *ABCD* matrix is $\begin{bmatrix} 1 & 0 \\ -j & 1 \end{bmatrix}$.

The *ABCD* matrix of the new design of HCFM shown in Fig. 4.6(a) in odd mode is shown in (4.7).

$$\begin{bmatrix} A & B \\ C & D \end{bmatrix} = \begin{bmatrix} 1 & 0 \\ -j & 1 \end{bmatrix} \begin{bmatrix} 0 & j \\ j & 0 \end{bmatrix} \begin{bmatrix} 0 & jK'_{01} \\ \dfrac{j}{K'_{01}} & 0 \end{bmatrix} \begin{bmatrix} 0 & j \\ j & 0 \end{bmatrix} \begin{bmatrix} 1 & 0 \\ -jK_{02} & 1 \end{bmatrix} = \begin{bmatrix} \dfrac{-K_{02}}{K'_{01}} & \dfrac{-\mathrm{j}}{K'_{01}} \\ \dfrac{\mathrm{j}K_{02}}{K'_{01}} - jK'_{01} & \dfrac{-1}{K'_{01}} \end{bmatrix} \quad (4.7)$$

In (4.7), $\begin{bmatrix} 1 & 0 \\ -jK_{02} & 1 \end{bmatrix}$ is the *ABCD* matrix for the coupling section between two bandpass filters in odd mode. The admittance of $\boldsymbol{\lambda}/8$ short-circuited stub is $Y = -jZ \tan \beta l = -jK_{02} * 1 = -jK_{02}$. According to Fig. 4.5, the *ABCD* matrix is $\begin{bmatrix} 1 & 0 \\ -jK_{02} & 1 \end{bmatrix}$.

The two *ABCD* matrices are also proven to be equal when (4.4) and (4.5) are satisfied.

In other words, the new structure will then have the same responses as a conventional design when (4.4) and (4.5) are satisfied.

Next step is to implement the concept in different cavity resonator filter technologies. We build the circuit model in ADS and the 3D structure in EM simulator, HFSS. The design process of the HCFM follows similar steps as described in the previous chapter. The circuit model in ADS serves as a coarse model and the 3D structure built in HFSS serves as the fine model. The parameter exaction techniques, such as those used in space mapping optimization, is used to aid the optimization of the dimensional parameters.

For coupler in the new HCFM structure, Z_0 and Z_1 are the characteristic impedance of the branches. In order to simulate the coupler structure more accurately and efficiently in the circuit model, the three-branch coupler can be divided into two symmetric T-junctions as shown in Fig. 4.7. Each T-junction can be realized using an E-plane or H-plane waveguide junction, or coaxial transmission line junction. The junction is EM simulated and built into the circuit model.

The initial values for L_1 is $\boldsymbol{\lambda}/4$, L_2 is $\boldsymbol{\lambda}/4$, K'_{01} is$\sqrt{2} * K_{01}$, and K_{02} is $K_{01}{}^2$. Z_0 and Z_1 can both be set as 1 for simplicity. Note that Z_1 may be assigned other values if needed. For example, if Z_1 =1.2 instead, $K'_{01} = 1.2 * \sqrt{2} * K_{01}$. L_1 and L_2 can also be assigned different lengths to make the design physically realizable. Furthermore, it can be shown that when the distance between two filters, L_2, changes by half wavelength, the responses remain the same if the coupling between two filters, K_{02}, is changed to -K_{02}. These characteristics make the new design of HCFM very flexible in practical implementation.

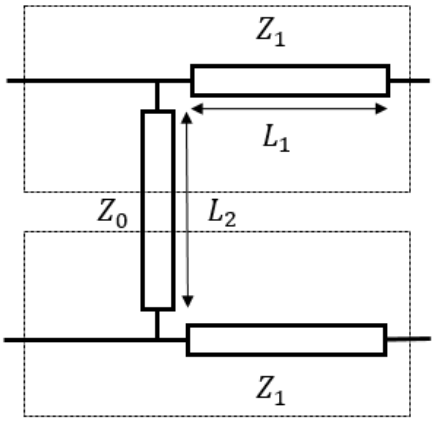

Figure 4.7. The three-branch coupler consisting of two T-junctions.

In the next part of this chapter, the new design concept is demonstrated in four different cases. Implementation of the new HCFM is realized using waveguide filters, dielectric resonator filters, and coaxial cavity filters. These three types of filters are the most frequently used cavity resonator filters in wireless and satellite applications. Moreover, the coupler structure in the design can take the forms of E-plane waveguide junction, H-plane waveguide junction, and coaxial transmission line junction.

4.2 Case 1: 3-pole Filter HCFM with Center Frequency Tunable from 12~12.4 GHz

In the first design, the branch lines of the coupler and the filters are implemented using rectangular waveguide. By adding a waveguide iris between two resonators, we can achieve the inter-resonator coupling between two filters.

We built the two 3-pole passband filters and the branch lines using the half-height WR-75 waveguide. Each resonator of the filters operates at TE102 mode.

The structure of the T-junction shown in Fig. 4.7 is built using an H-plane rectangular waveguide T-junction as shown in Fig. 4.8.

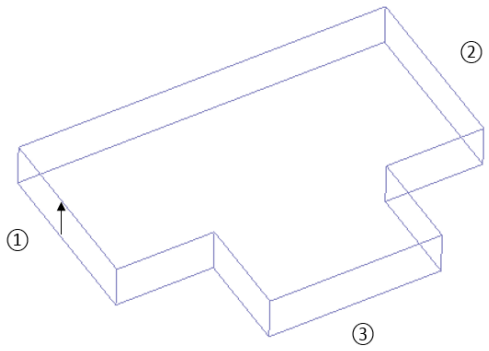

Figure 4.8. Structure of an H-plane rectangular waveguide T-junction.

As we know, the ideal 3dB coupler in the conventional design can divide the power inserted from port 1 equally into port 2 and port 3. However, with the existing waveguide T-junction, the power entered from port 1 cannot be divided equally to port 2 and port 3, which causes difficulty in the optimization to realize the ideal responses in the circuit model.

The problem is solved by adding an extra metal post at the center of the waveguide T-junction as shown in Fig. 4.9. By optimizing the size of the metal post, the equal power output between port 2 and port 3 can be realized. For S parameters of the T-junction with the metal post, S_{21} is equal to S_{31} and S_{11} is equal to S_{33}. The S parameters of the T-junction in Fig 4.9 is shown in Fig. 4.10.

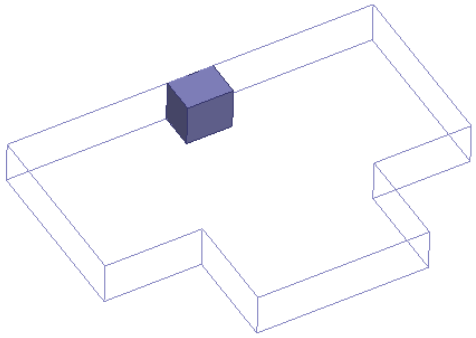

Figure 4.9. Waveguide T-junction with an extra metal post.

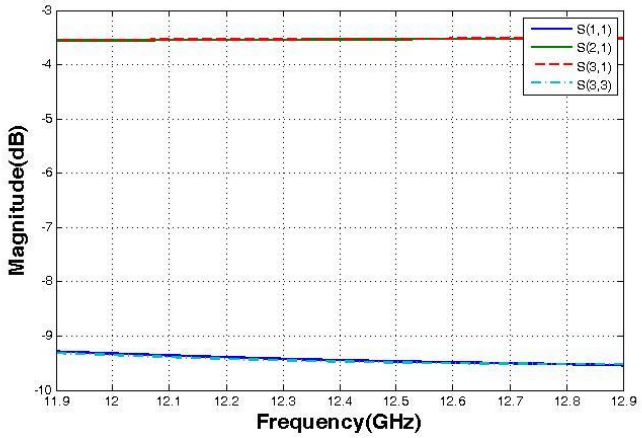

Figure 4.10. S parameters of the T-junction with an extra metal post.

In the design process of a new HCFM, we first optimize the design parameters in the coarse model in ADS to satisfy the original requirements. The circuit model of the part

before first waveguide resonator for the new HCFM structure is shown in Fig. 4.11. The T-junctions are EM simulated in HFSS in order to have more accurate results. The waveguide branch line of the coupler and the waveguide resonators are all simulated using S-parameters of waveguide transmission lines. Coupling sections are represented in *ABCD* matrices, which include the input/output coupling, the inter-resonator coupling in single filter and the coupling between two filters. The two identical bandpass filters are built using two ideal 3-pole rectangular waveguide filters.

In the ADS, we set the distance between two filters, which is also the length between port 1 and port 4 in a 3dB coupler, as L_2, and the length of branch between port 1 and port 2 in a 3dB coupler as L_1. L_2 needs to be larger than the width of the waveguide, which is 0.75in, to make the design physically realizable. The inter-resonator coupling is set as K_{02}. All characteristic impedances of the transmission lines are set as 1 in the circuit model. As a result, we need to enlarge the input/output coupling by $\sqrt{2}$. After tuning the length of L_1, L_2 and the coupling between two filters K_{02}, we can realize the required S parameters. These parameters serve as the optimal coarse model in our design process.

Next, the two identical 3-pole waveguide filters are firstly optimized in HFSS following the same design process of a 3-pole dielectric resonator filter in chapter 3. The initial size of the waveguide iris for coupling between two filters K_{02} can be calculated using a two-coupled resonator structure in HFSS. Two resonators are identical and each of them is from the two filters. The coupling K_{02} can be calculated by the two resonant frequencies f_e and f_m from eigenmode simulation in HFSS as follows:

$$K_{02} = \frac{({f_e}^2 - {f_m}^2)}{({f_e}^2 + {f_m}^2)} \tag{4.8}$$

The initial values for the lengths of the coupler branches can be set as L_1 and L_2 from the optimal coarse model in ADS.

After tuning the length of the branch lines and also the coupling between two filters, we can achieve the HCFM function in our new design both in ADS and HFSS. The optimal S parameters in ADS are shown in Fig. 4.12. The structure of the HCFM in EM simulator, HFSS, is shown in 4.13 and the S parameters from HFSS after tuning are shown in Fig. 4.14.

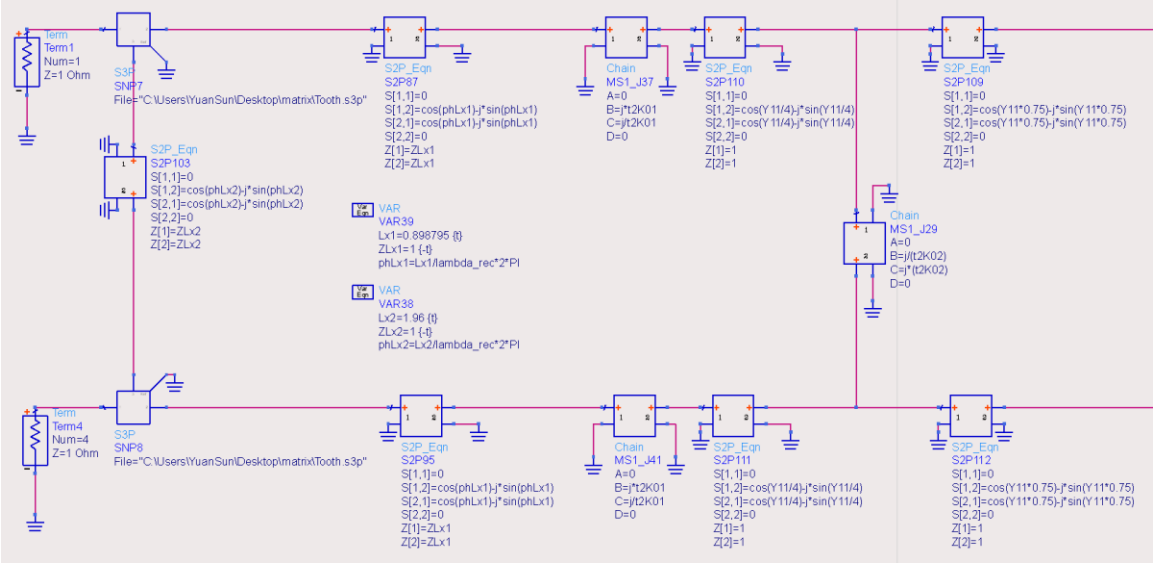

Figure 4.11. The circuit model of the part before first waveguide resonator for the new HCFM structure.

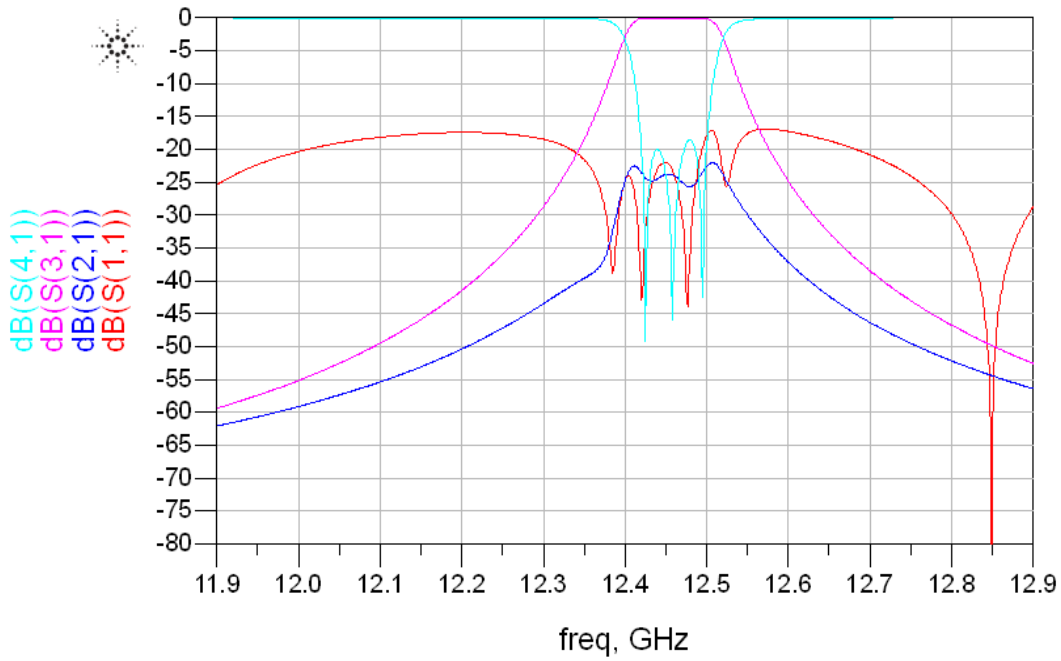

Figure 4.12. S parameters in ADS of the HCFM with 3-pole filters operating at 12.46GHz.

The center frequency of the HCFM is at 12.46GHz and the bandwidth is 85MHz. The height of the cavities is 0.1875in, which is half height of the WR-75 waveguide. The L_1 in HFSS is 0.8in and L_2 in HFSS is 1.96in. In HFSS, L_2 is the distance between the centers of the two filters. L_1 is the length of the waveguide from center of the T-junction to the input coupling iris. The L_1 in ADS is 0.898in and L_2 in ADS is 1.96in. K'_{01} is 0.258 in ADS and K_{02} is 0.031 in ADS.

As shown in the Fig 4.12 and Fig. 4.14, the S_{21} and S_{11} are below -18dB over the entire frequency range of interest. The S_{31} and S_{41} function as the S_{21} and S_{11} in a single filter. In conclusion, with inputs at port1 and the port 2 terminated with matched load, the out-of-

band channels will emerge from port 4 and the in-band channel will emerge at port 3. We achieve the HCFM function successfully with the new design of HCFM.

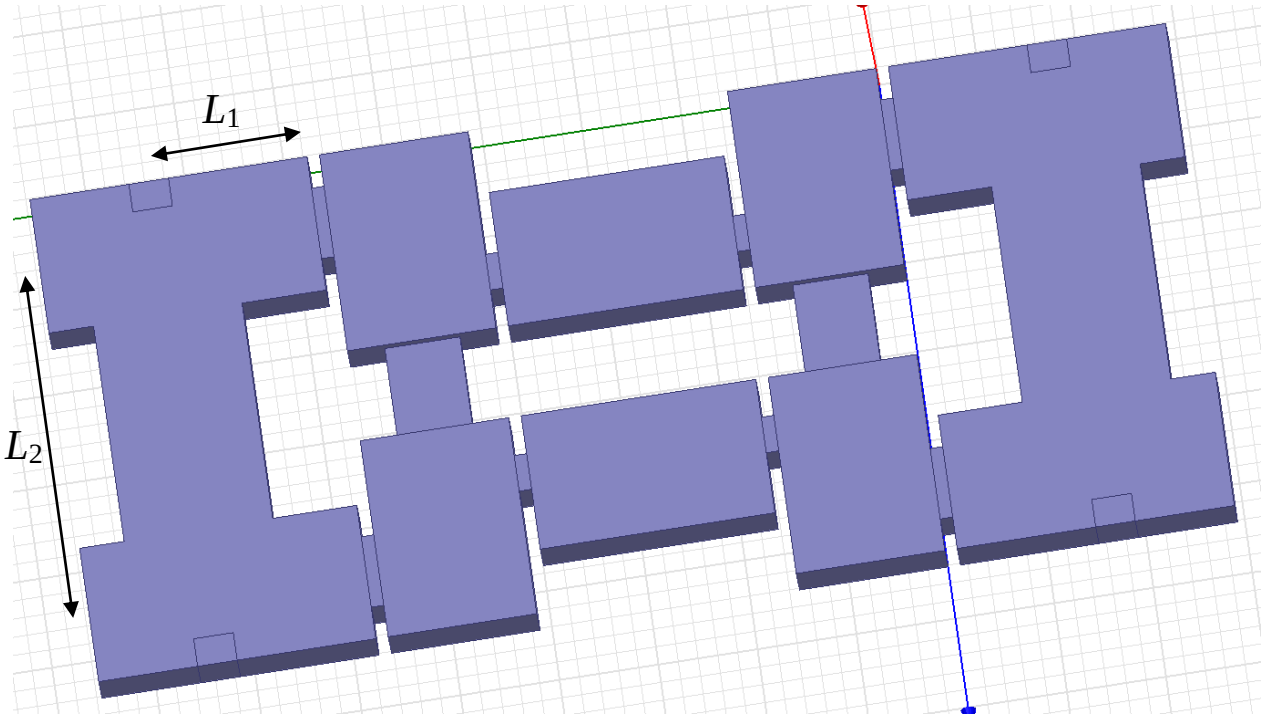

Figure 4.13. Structure of the HCFM realized with two 3-pole waveguide filters in HFSS.

The structure of the new design of HCFM achieves more than 30% reduction in size compared to the conventional HCFM. In conventional designs of the HCFM, we need to extend the waveguide coupler on both sides of the structure shown in Fig. 4.13.

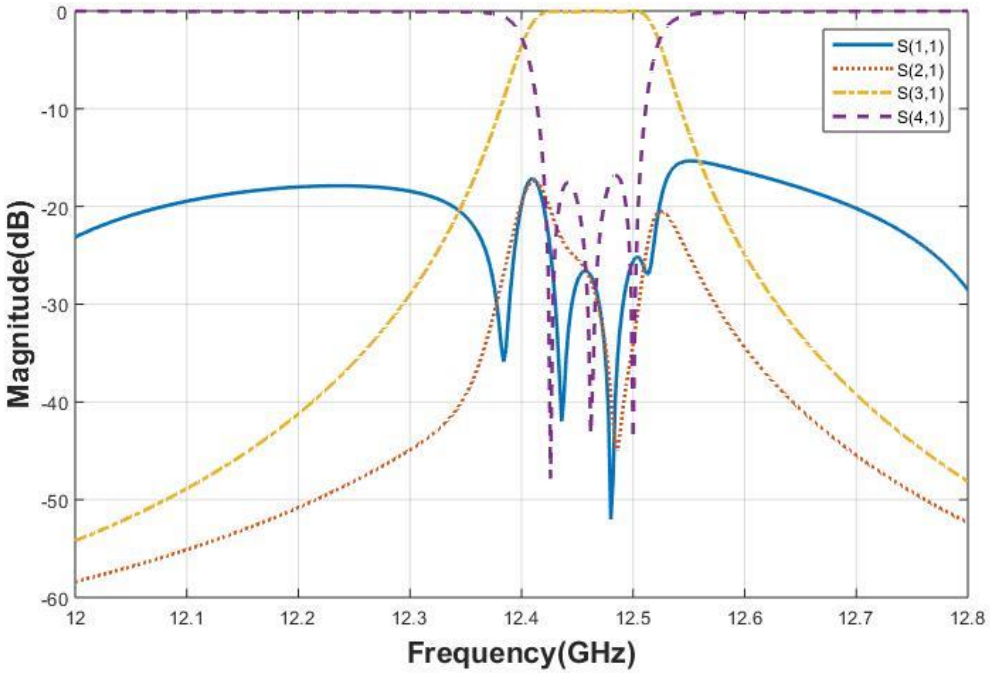

Figure 4.14. S parameters in HFSS of the HCFM realized with two 3-pole waveguide filters operating at 12.46GHz.

Tunability of the new HCFM design

Next, we demonstrate the tunability of the new HCFM design. Tuning screws have been widely used to adjust filter responses [60-61]. By adding screws in both cavity resonators and waveguide couplers in the structure in Fig. 4.13, the center frequency can be tunable in the physical model.

The structure of the new HCFM with tuning screws in HFSS is shown in Fig. 4.15. We put two screws in each waveguide resonator of the two filters for tuning of the filter center frequency. And four screws are put in each coupler structure to tune the electrical lengths of each waveguide section. The dimeter of the screws in our design is 0.086in, and the lengths of the screws are tuned. In this case, the center frequency changes from12.46GHz

to 12.08GHz. The S parameters of the 3-pole filter HCFM with tuning screws are shown in Fig.4.16. Moreover, S_{31} and S_{41} figures in two structures are compared in Fig.4.17.

As shown in Fig 4.16, we can still achieve the HCFM function in our design. The center frequency is at 12.08GHz and the band width is still 85MHz. Only the S_{11} figure becomes slightly worse in the right side of the passband, which can be improved by adding tuning screws in the coupling irises as well. In conclusion, we achieve the tunability of the new design of HCFM by adding several tuning screws in the cavity resonator and waveguide coupler.

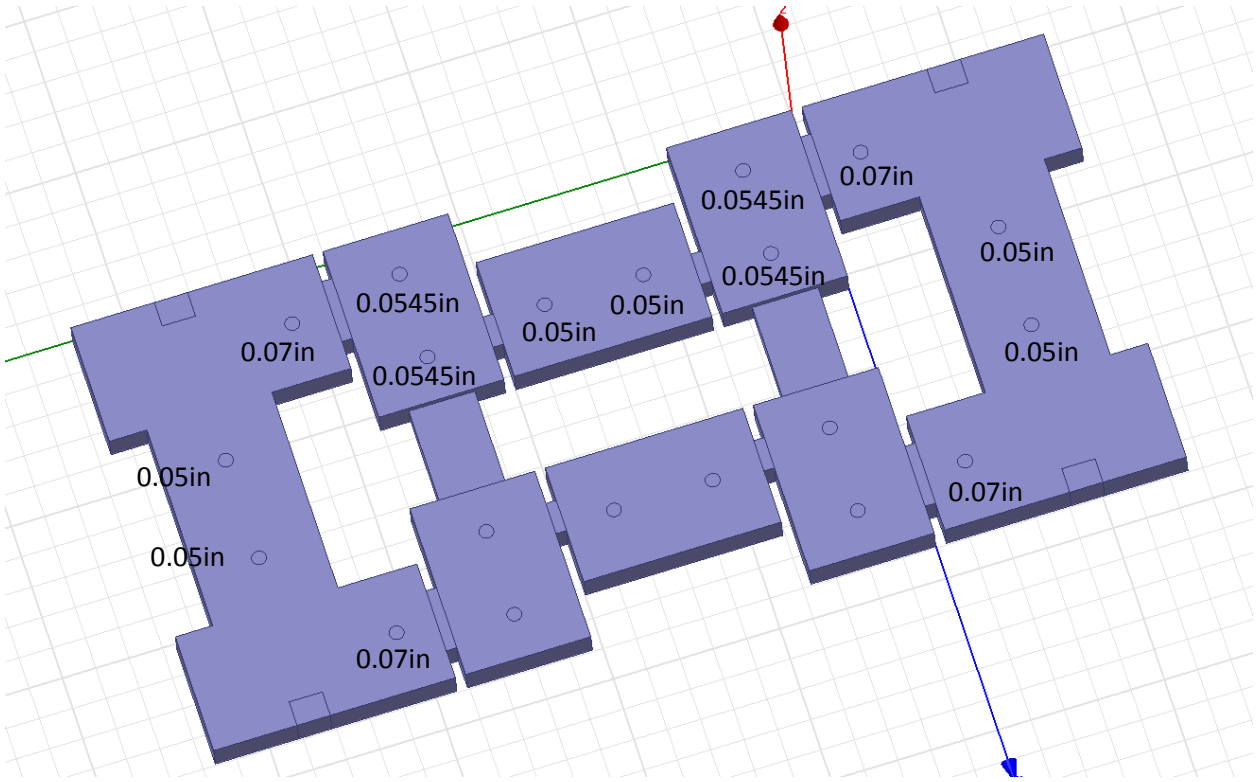

Figure 4.15. Structure of a 3-pole filter HCFM with tuning screws in HFSS.

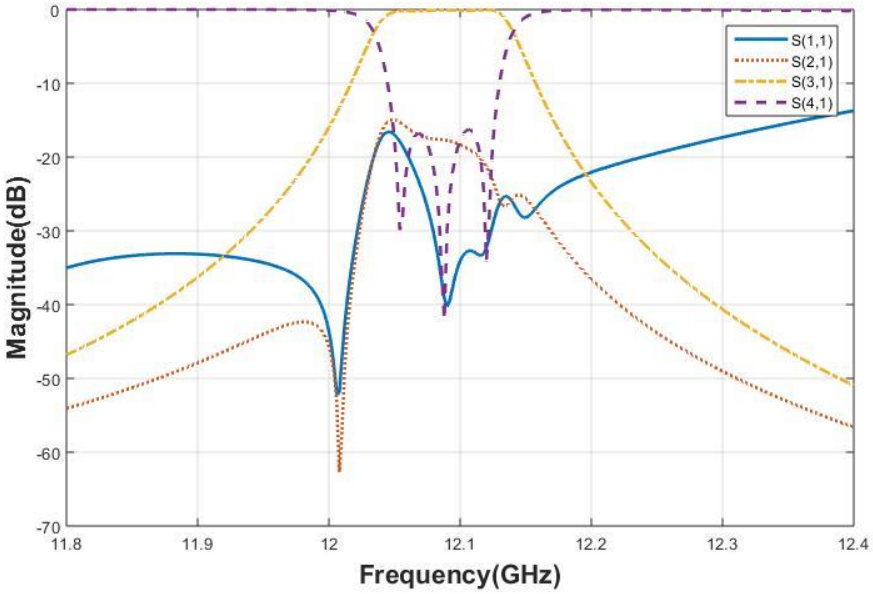

Figure 4.16. S parameters for a 3-pole filter HCFM with tuning screws in HFSS.

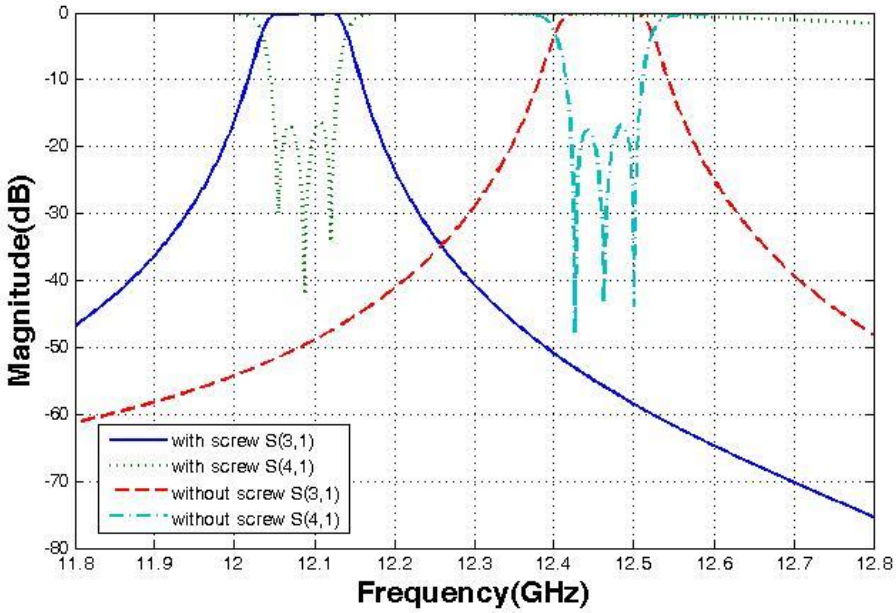

Figure 4.17 Comparison of S parameters for the two structures with and without tuning screws, showing the tuning range of the center frequency from12.46GHz to 12.08GHz.

The structure can be fabricated by dividing it into two parts: the main structure and the lid with tuning screws on it. The 3D structures for fabrication are shown in Fig. 4.18(a) and (b). The Fig. 4.18(a) shows the main structure without the lid on the top. It can be machined using copper or silver. The Fig. 4.18(b) shows the structure of the HCFM with tuning screws showing on the lid.

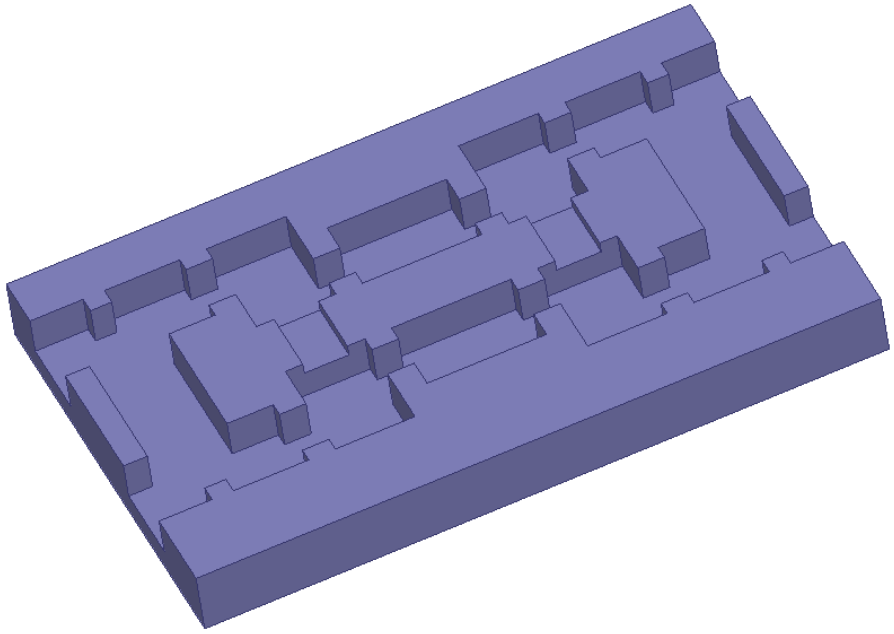

(a)

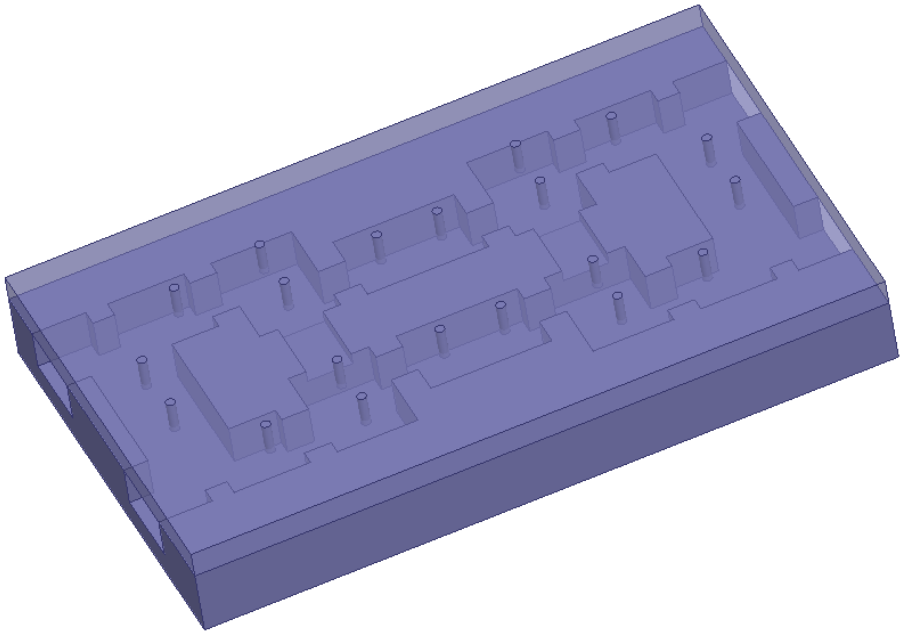

(b)

Figure 4.18. (a) The 3D view of the structure without the lid, and (b) the 3D view of the structure with tuning screws showing on the lid.

4.3 Case 2: 5-pole Filter HCFM Centered at 17.4 GHz

In case 2, we design a 5-pole filter HCFM with a relatively large bandwidth.

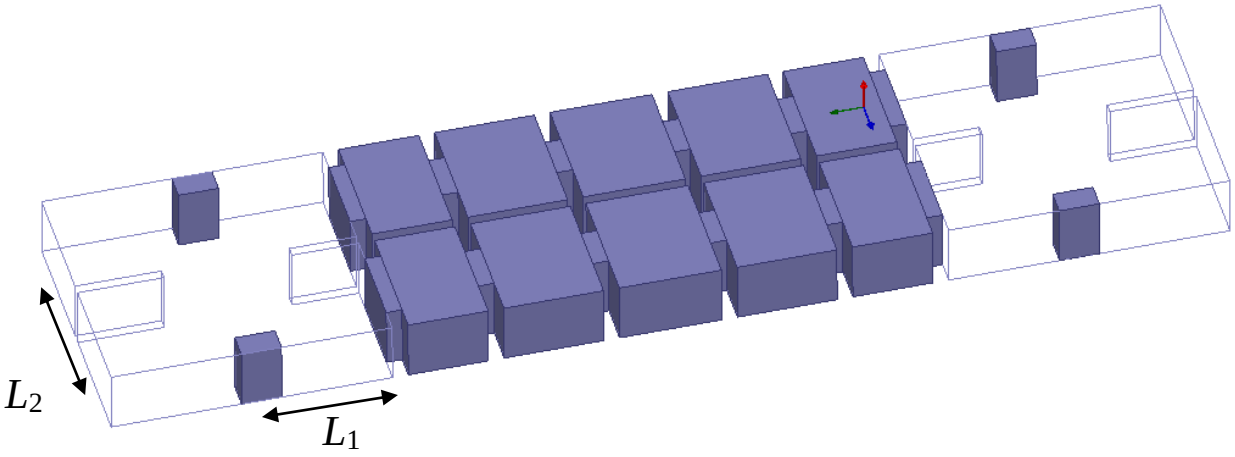

Figure 4.19. Structure of the HCFM with 5-pole filters in HFSS.

The structure of the HCFM realized with two 5-pole waveguide filters is shown in Fig. 4.19. Two 5-pole rectangular waveguide filters are used in the design, the center frequency for one single filter is 17.4GHz and the band width is 700MHz. The coupler in the design is built by two H-plane waveguide junctions.

The two 5-pole passband filters and the branch lines are built using WR-51 waveguide. Each resonator of the filters operates at TE101 mode.

The circuit model built in ADS and the S parameters in ADS are shown in Fig. 4.20 and Fig. 4.21.

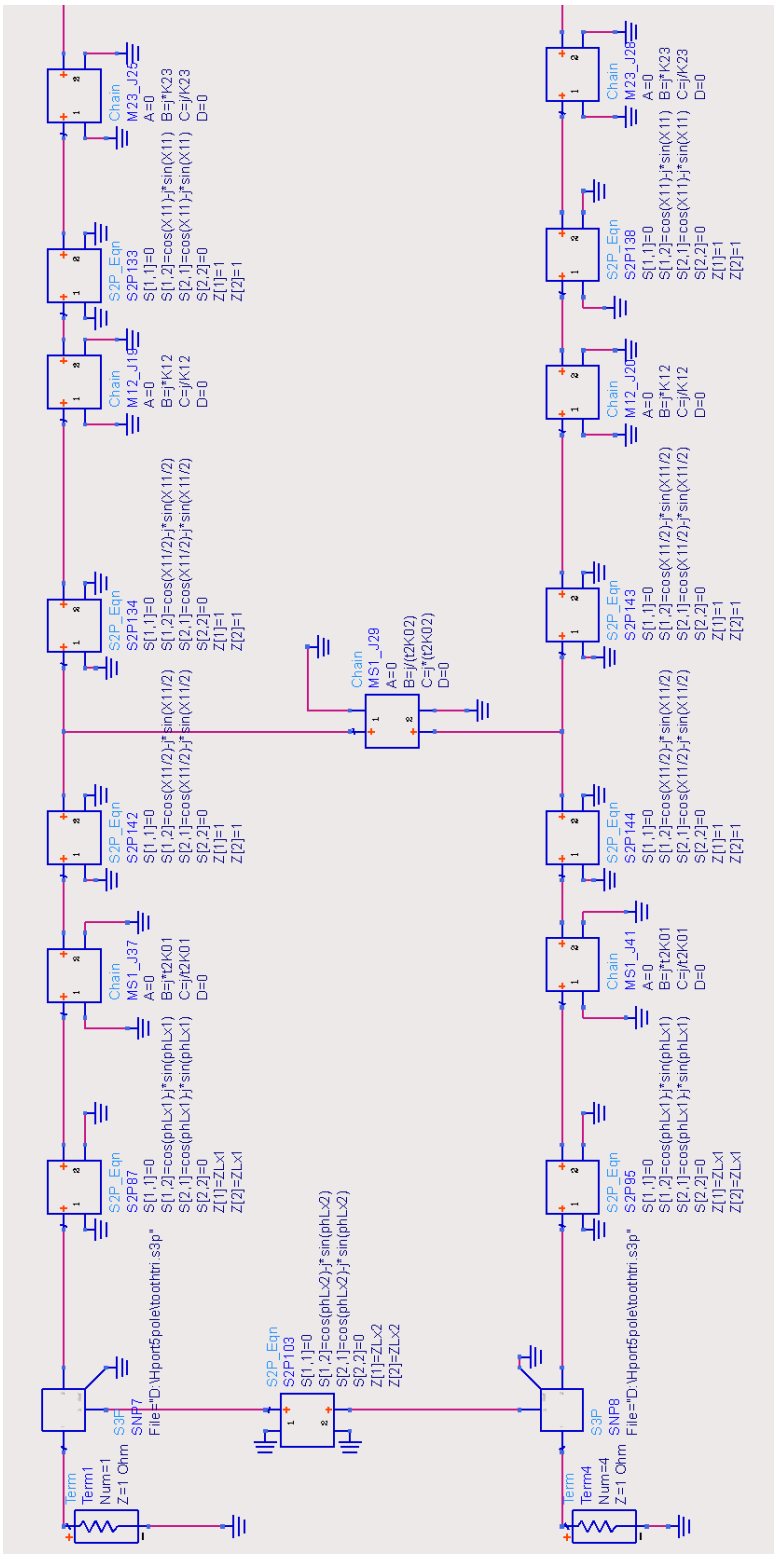

(a)

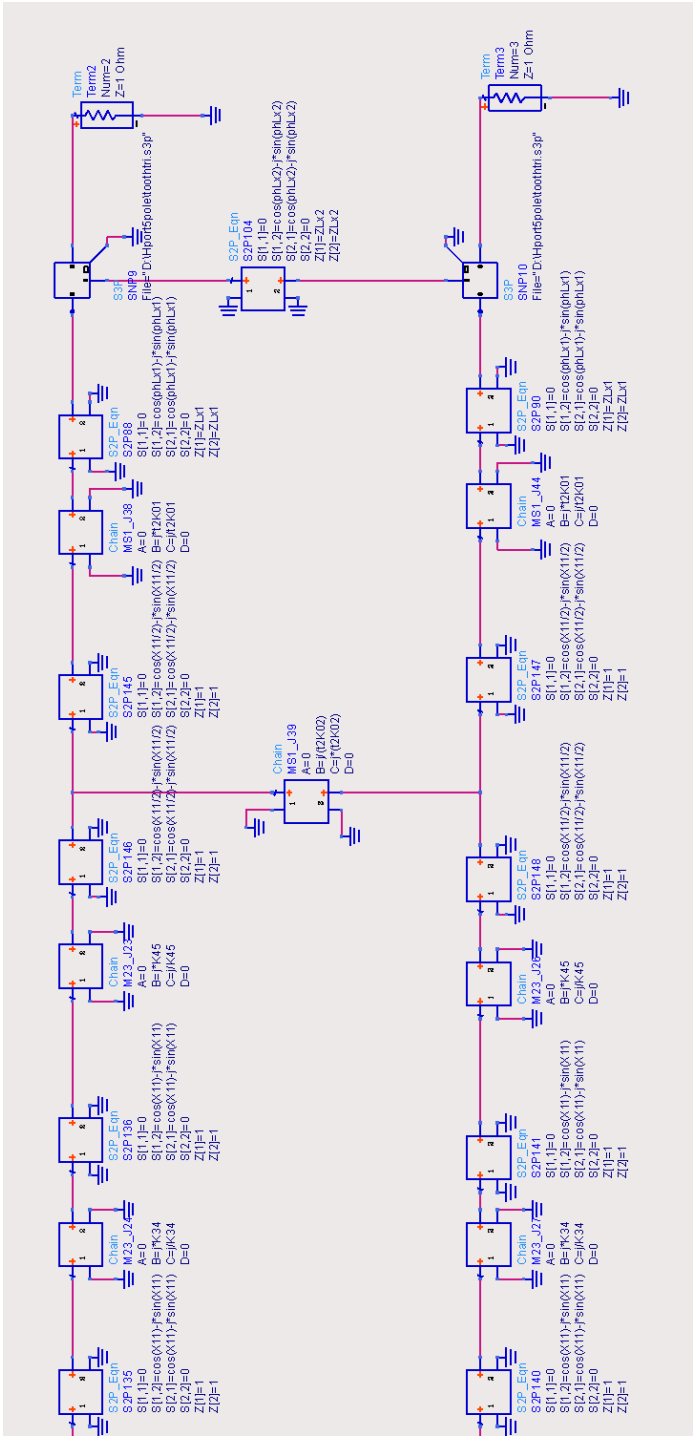

(b)

Figure 4.20. Circuit model of the HCFM with 5-pole filters: (a) the left half, and (b) the right half.

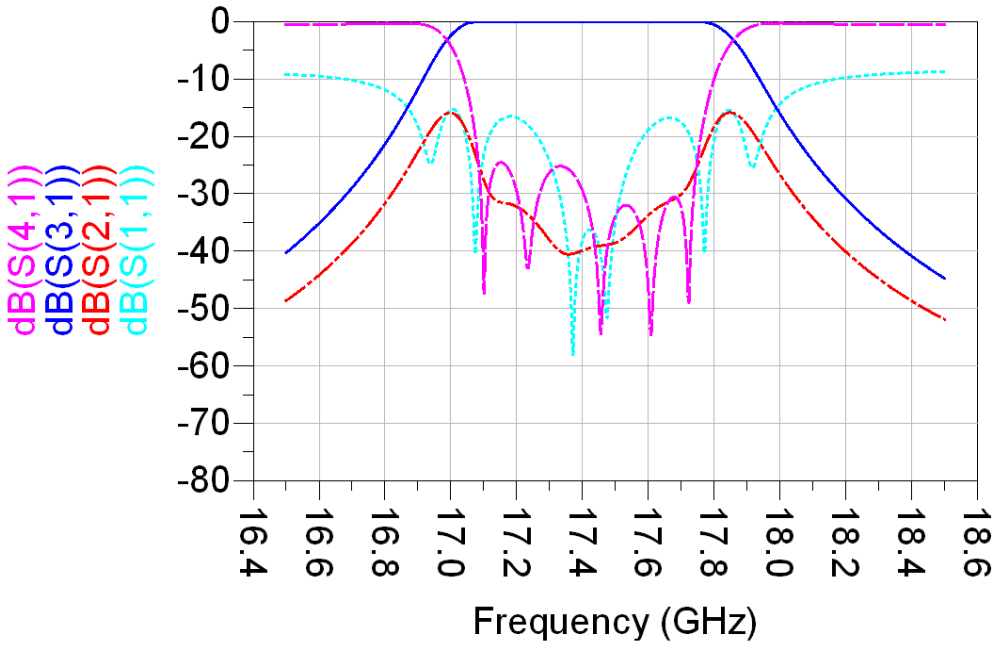

Figure 4.21. S parameters of the HCFM with 5-pole filters in ADS.

The EM simulated S parameters of the HCFM with 5-pole filters are shown in Fig. 4.22, showing a center frequency of 17.4 GHz and a bandwidth around 700MHz. The L_1 in HFSS is 0.522in and L_2 in HFSS is 0.55in. In ADS, the L_1 is 0.66in and L_2 is 0.52in. K'_{01} is 0.743 and K_{02} is 0.272.

As we can see in Fig.4.21 and Fig 4.22, the S_{11} from both ADS and HFSS is below -10 dB instead of -20 dB. This happens when we want to achieve a large bandwidth with the structure. This limitation needs further investigation and the S_{11} needs further tuning.

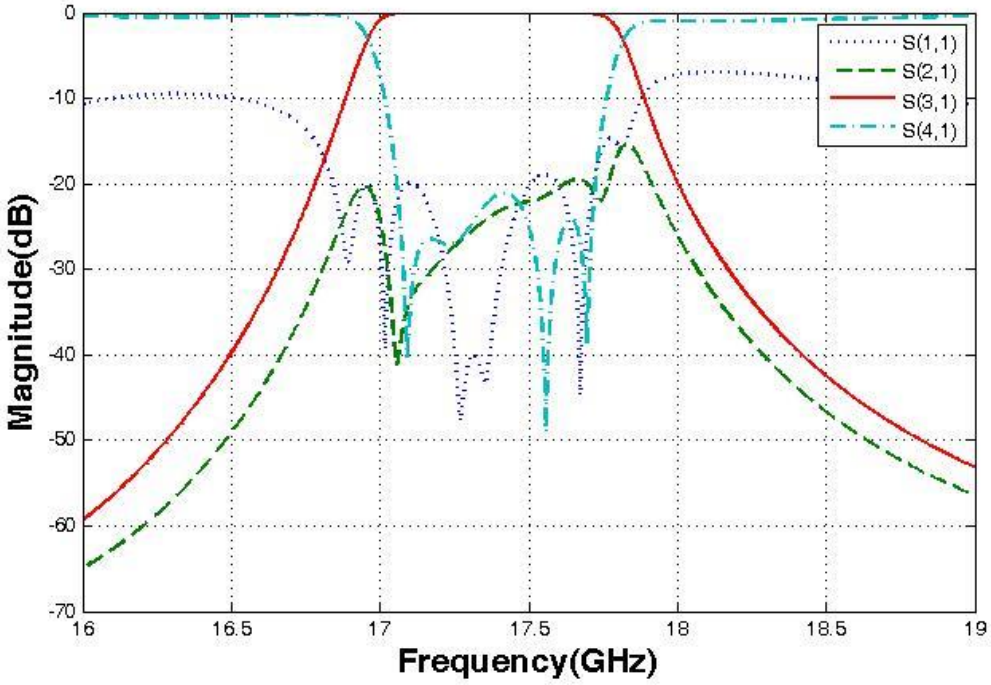

Figure 4.22. EM simulated S parameters of the HCFM with 5-pole filters using HFSS.

Another finding is that when we terminate one of the ports in HCFM with a short circuit, the results are not affected, as shown in Fig. 4.23. When port 2 in a HCFM is terminated with a short circuit, the S parameters in ADS are shown in Fig. 4.24. As we can see, the $S_{11,}$ S_{31} and S_{41} remain the same as in Fig. 4.21. When port 4 in a HCFM is terminated with a short circuit, the S parameters in ADS are shown in Fig. 4.25. The S_{21} and S_{31} remain the same as in Fig. 4.21, the S_{11} is the same as S_{41} in Fig. 4.21, which means the out-band signals will emerge from port 1 in this situation.

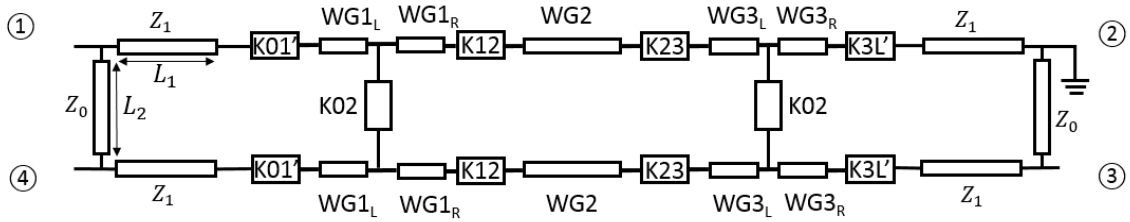

Figure 4.23. Structure of the HCFM with port 2 terminated with a short circuit.

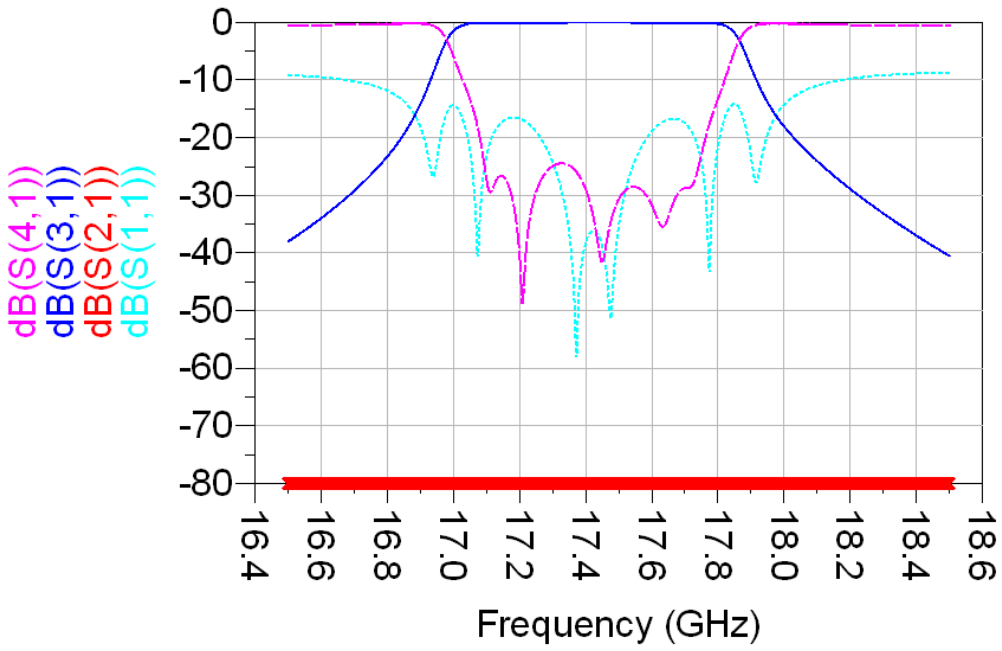

Figure 4.24. S parameters of the 5-pole filter HCFM in ADS with port 2 terminated with a short circuit.

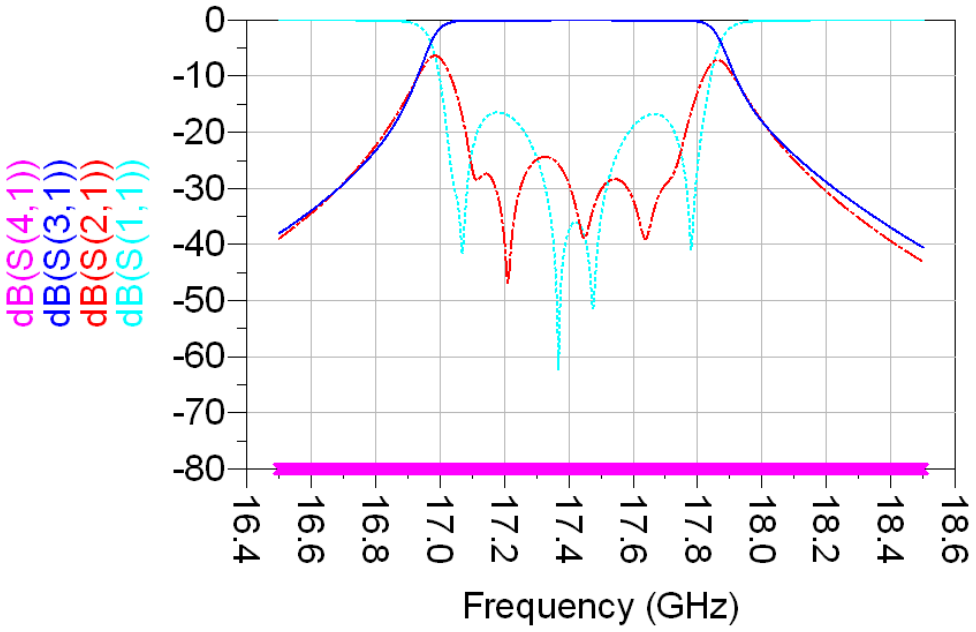

Figure 4.25. S parameters of the 5-pole filter HCFM in ADS with port 4 terminated with a short circuit.

4.4 Case 3: Design of HCFM with E-plane Junction

Designs in case 1 and case 2 all use the H-plane waveguide junctions to achieve the coupler branch lines. We can also use the E-plane T-junction in the design. The structure of an E-plane T-junction is shown in Fig 4.26. It is also built using the half height WR-75 waveguide as in case 1.

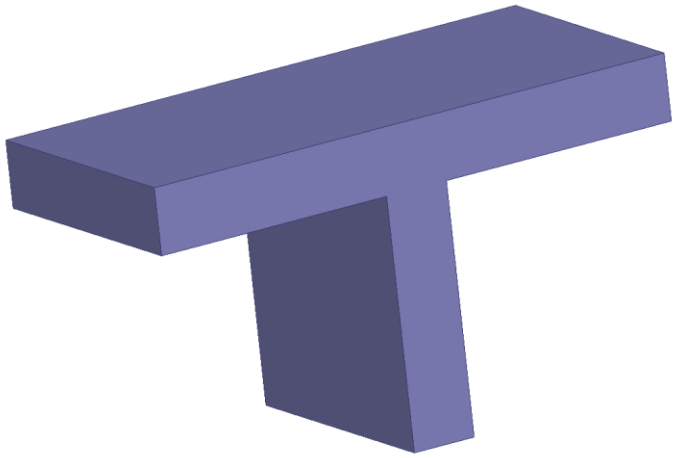

Figure 4.26. E-plane T-junction.

The circuit model built in ADS for the HCFM with E-plane T-junction is almost the same as the HCFM built with H-plane T-junctions. The only difference is the EM simulated T-junction.

As discussed earlier, when the distance between two filters, L_2, changes by half wavelength, the sign of the coupling between two filters, K_{02}, need to change, i.e. either from negative coupling to positive coupling or from positive to negative, so that the responses remain the same.

This characteristic of the new HCFM allows certain flexibility in the physical realization of the design. Two examples are built in HFSS using the E-plane T-junctions for demonstration, as shown in Fig. 4.27 and Fig. 4.28. The bandpass filters are 3-pole filters using half height WR-75 waveguides and each resonator operates at TE101 mode. The coupling section between two filters are realized by the irises.

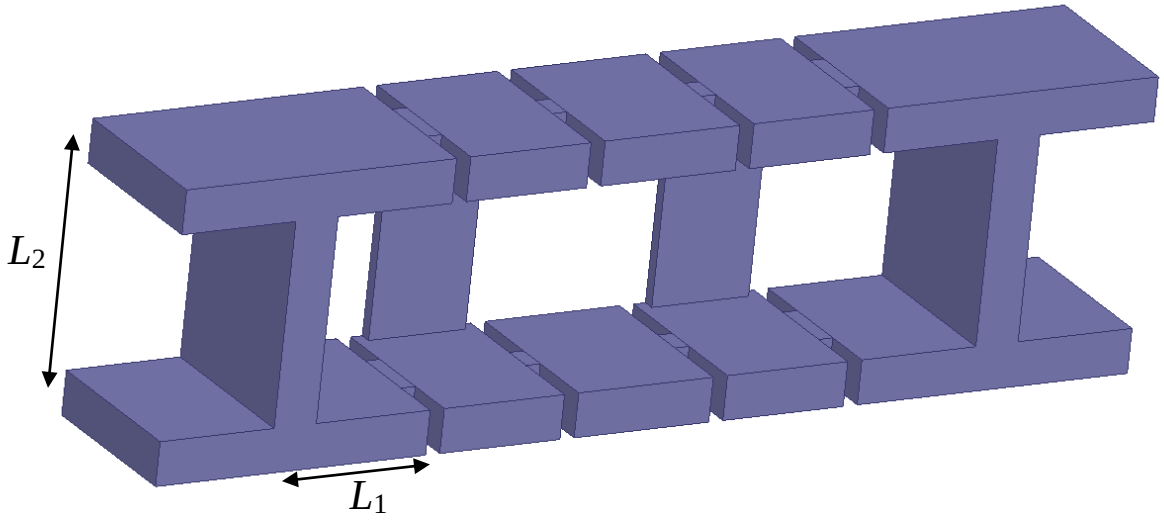

Figure 4.27. Structure of the HCFM with 3-pole filters, E-plane junction and positive inter-resonator coupling.

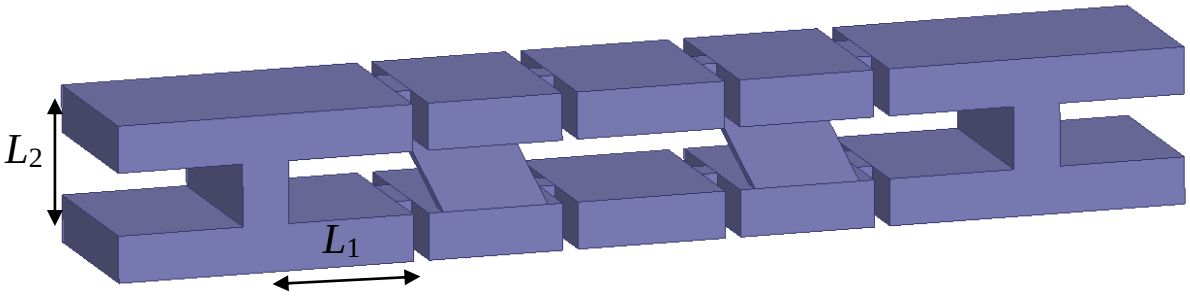

Figure 4.28. Structure of the HCFM with 3-pole filters, E-plane junction and negative inter-resonator coupling.

The EM simulated S parameters of the two structures are shown in Fig. 4.29 and Fig. 4.30. For the HCFM with positive coupling, the center frequency is at 12.415GHz and the band width is 70MHz. The L_1 in ADS is 0.625in and L_2 in ADS is 1.053in. K'_{01} is 0.279 in ADS and K_{02} is 0.044 in ADS. The L_1 in HFSS is 0.6in and L_2 in HFSS is 1.053in. For the HCFM with negative coupling, the center frequency is also at 12.415GHz and the band width is 70MHz. The L_1 in ADS is 0.625in and L_2 in ADS is 0.438in. K'_{01} is 0.279 in ADS and K_{02} is -0.044 in ADS. The L_1 in HFSS is 0.6in and L_2 in HFSS is 0.438in.

The distance between two filters, which is L_2, are different by $\boldsymbol{\lambda}/2$ because the coupling between two filters change from positive sign to negative sign. For the structure in Fig 4.28, the sign of the coupling between two filters is negative, and the design is more compact. However, the structure is more complicated and more difficult to fabricate. For the structure in Fig. 4.27, the sign of the coupling between two filters is positive. The design is bulky. But the coupling section is easier to fabricate.

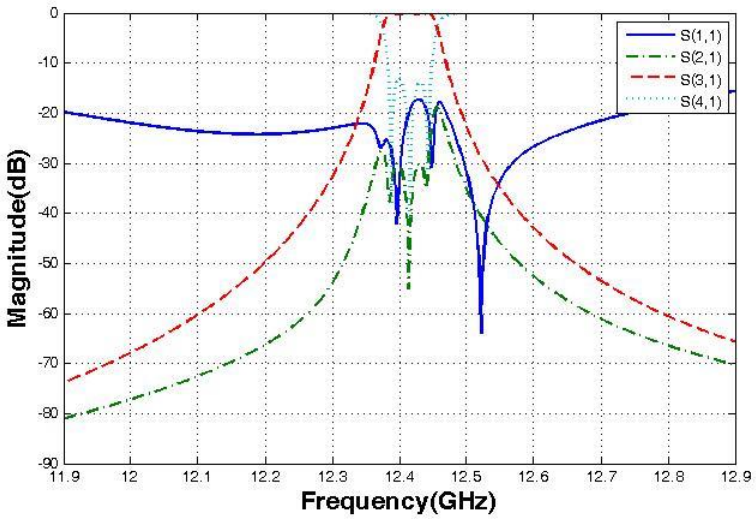

Figure 4.29. EM simulated S parameters of the HCFM with E-plane junction and positive inter-resonator coupling.

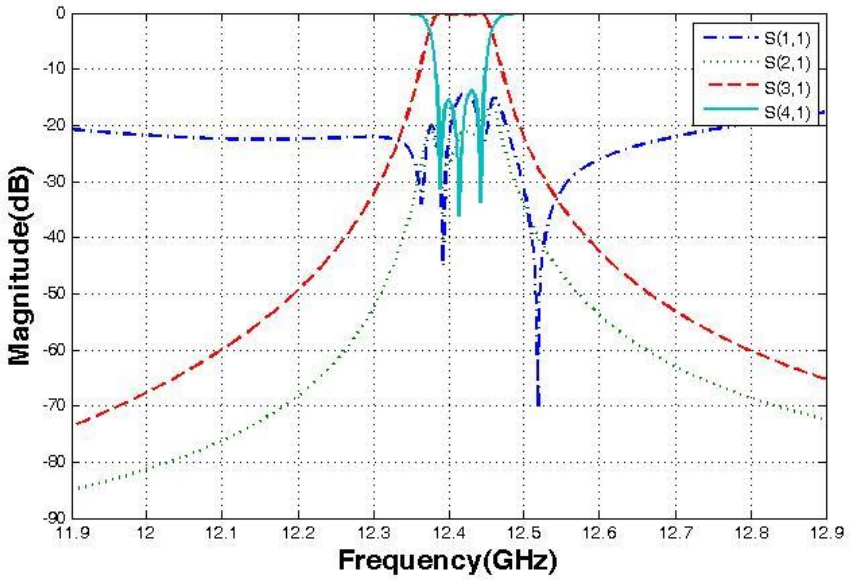

Figure 4.30. EM simulated S parameters of the HCFM with E-plane junction and negative inter-resonator coupling.

4.5 Case 4: Design of HCFM with Coaxial Transmission Line Coupler and Different Cavity Resonator Filters

The branch lines of the coupler can also be achieved by coaxial transmission line [62]. In addition, the two identical filters in the HCFM can take forms of other cavity resonator filters, such as coaxial cavity filter and dielectric resonator filter.

We built the two 3-pole passband filters using two identical coaxial cavity filters. By opening irises and adding coupling wires in two resonators, we can achieve the inter-

resonator coupling between two filters. The structure of the HCFM is shown in Fig 4.31. The coupler is realized using the coaxial transmission line junctions.

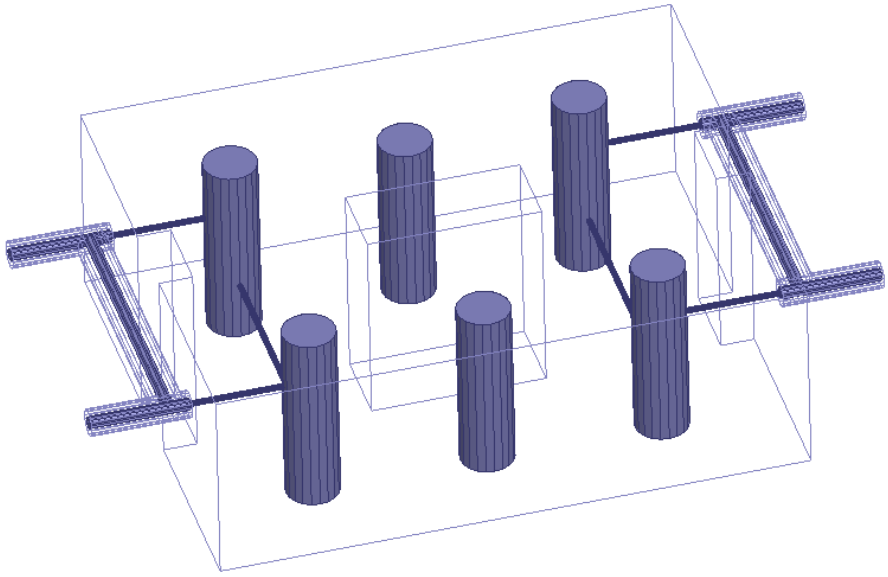

(a)

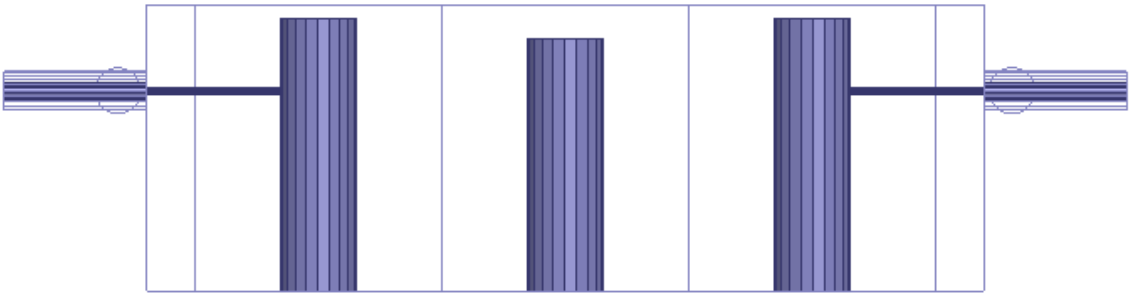

(b)

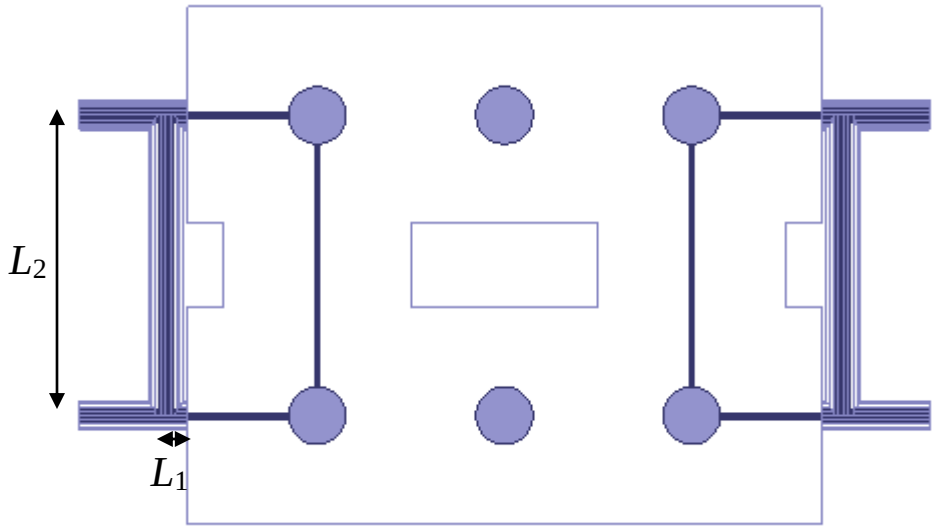

(c)

Figure 4.31. Structure of the HCFM with 3-pole coaxial cavity filters and coaxial transmission line junctions: (a) perspective view, (b) side view, and (c) top view.

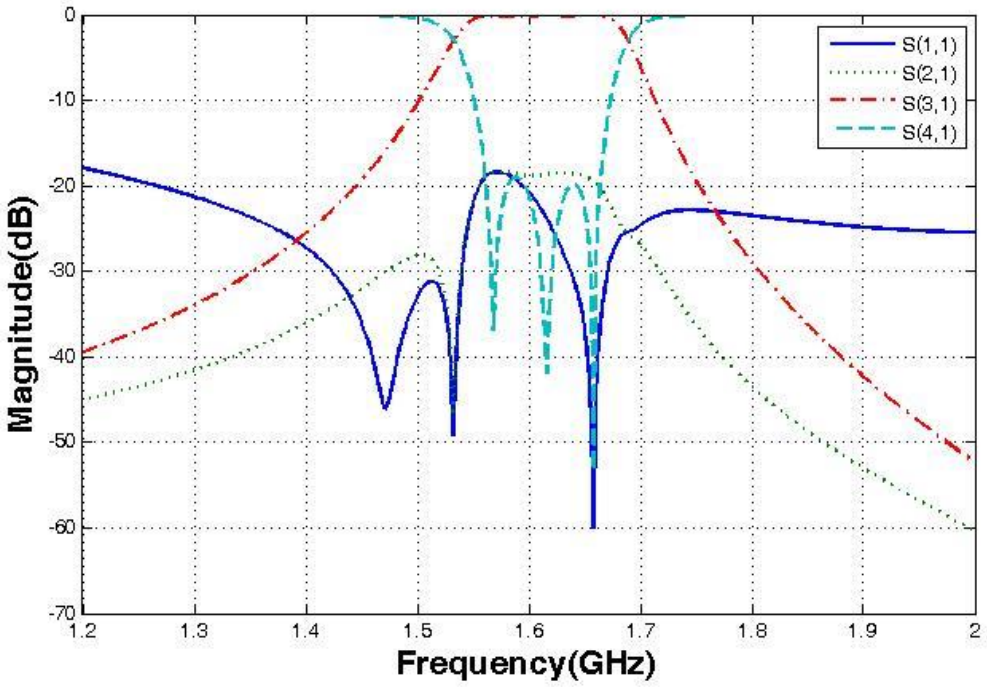

Figure 4.32. EM simulated S parameters of the HCFM with 3-pole coaxial cavity filters and coaxial transmission line junctions.

The EM simulated S parameters of the structure in Fig. 4.31 is shown in Figure 4.32. As can be seen, the structure achieves the function of an HCFM. The center frequency is at 1.6GHz, the bandwidth is 100MHz. The L_1 in HFSS is 0.15in and L_2 in HFSS is 2.08in. The L_1 in ADS is 1.935in and L_2 in ADS is 2.09in. K'_{01} is 0.41 in ADS and K_{02} is 0.089 in ADS.

Another configuration of the HCFM is to use dielectric resonator filters. The coupler is also implemented using coaxial transmission lines. The structure is shown in Fig. 4.33.

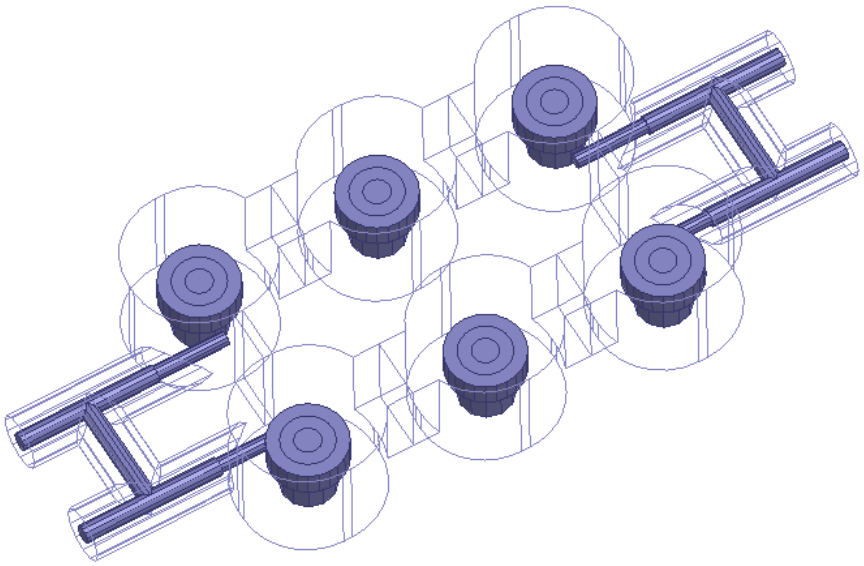

(a)

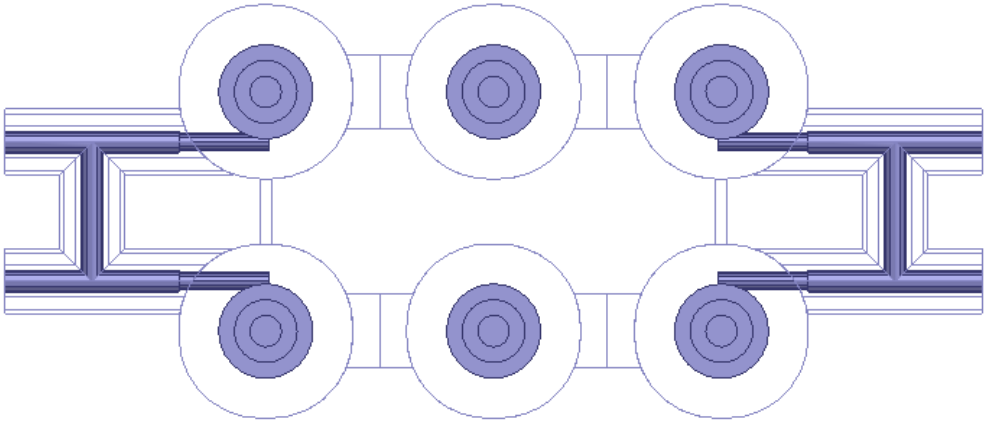

(b)

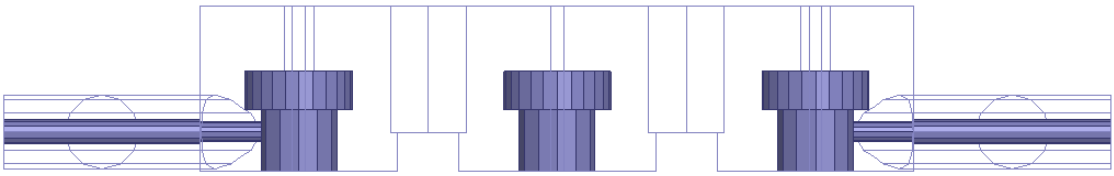

(c)

Figure 4.33. Structure of the HCFM with 3-pole dielectric resonator filters and coaxial transmission line junction (a) perspective view, (b) top view, and (c) side view.

The EM simulated S parameters of the structure in Fig. 4.33 is shown in Figure 4.34. As can be seen, the structure achieves the function of an HCFM. The center frequency is at 12.8GHz, and the bandwidth is 30MHz. The L_1 in HFSS is 0.2in and L_2 in HFSS is 0.32in.

The L_1 in ADS is 0.23in and L_2 in ADS is 0.32in. K'_{01} is 0.104 in ADS and K_{02} is 0.0058 in ADS.

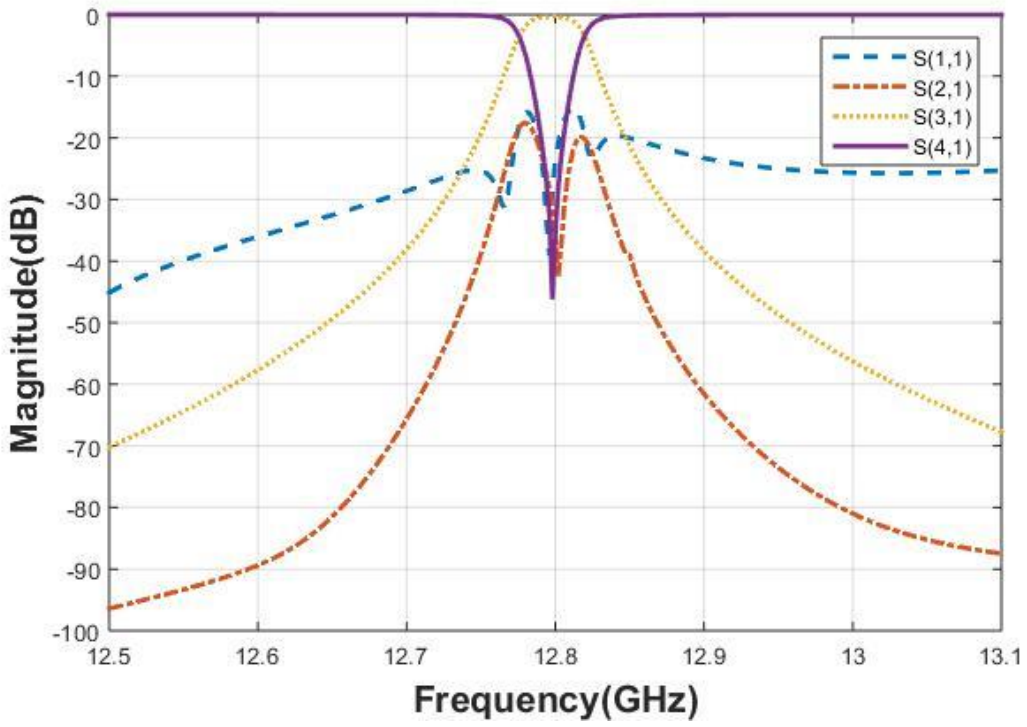

Figure 4.34. EM simulated S parameters of the HCFM with 3-pole dielectric resonator filters and coaxial transmission line junctions.

4.6 Summary

In chapter 4, we first introduce the design concept of a new HCFM structure. The even-odd mode decomposition technique is used to prove that by using the inter-resonator couplings between two filters to replace one branch in a 3dB hybrid coupler, we can achieve the same responses of a conventional design and make the design of HCFM more

compact. A number of examples are built both in ADS and HFSS. Implementation of the new design is realized using waveguide filters, dielectric resonator filters and coaxial cavity filters. Moreover, the coupler structure in the new design can take the forms of E-plane waveguide junction, H-plane waveguide junction, and coaxial transmission line junction.

It is demonstrated that using tuning screws in both cavity resonators and waveguide junctions, we achieve the tunability of the HCFM. In addition, one of the HCFM ports can be terminated in short circuit without affecting the results. It is further demonstrated that the responses of the HCFM remain the same if the distance between two filters changes by half wavelength, and at the same time the sign of the coupling between two filters changes, either from negative coupling to positive coupling or from positive to negative. Compared with conventional designs of HCFMs, all of the examples shown in this chapter achieve size reduction by decreasing the size of the couplers on both sides.

Chapter 5

Conclusion and Future Work

In this thesis, two types of compact microwave filter designs based on cavity resonators are developed.

A compact design of dual-band filter is presented first. By adding additional posts in the irises of a dielectric resonator filter, an extra evanescent mode filter can be achieved. The design concept of this dual passband filter has been proved in this thesis. The resulting filter is extremely compact, and the design method is straightforward.

In addition, a new design of HCFM is presented. We use the inter-resonator coupling between two filters to replace one branch in a 3dB hybrid coupler to make the design of HCFM more compact. Implementation of the new design is realized using waveguide filters, dielectric resonator filters and coaxial cavity filters. In all cases, the new structure preserves the responses of a conventional design. Moreover, by using tuning screws in both cavity resonators and waveguide junctions of the new design of HFCM, we achieve the tunability of the HCFM.

Some following aspects can be further investigated.

- Improve the spurious performance of the dual-band filter using DRF and evanescent mode filter;
- Improve the S parameters when using the new designed HCFM in a wide-band application; and
- Structures built in chapter 3 and chapter 4 can be fabricated and measured.

BIBLIOGRAPHY

[1] L.-C. Tsai and C.-W. Hsue, "Dual-band bandpass filters using equal-length coupled-serial-shunted lines and Z-transform technique," *IEEE Trans. Microw. Theory Techn.*, vol. 52, no. 4, pp. 1111-1117, Apr. 2004.

[2] C. F. Chen, T. Y. Huang, and R. B. Wu, "Design of dual- and triple-passband filters using alternately cascaded multiband resonators," *IEEE Trans. Microw. Theory Techn.*, vol. 54, no. 9, pp. 3550–3558, Sep. 2006.

[3] C. M. Tsai, H. M. Lee, and C. C. Tsai, "Planar filter design with fully controllable second passband," *IEEE Trans. Microw. Theory Techn.*, vol. 53, no. 11, pp. 3429–3439, Nov. 2005.

[4] J. T. Kuo and E. Shih, "Microstrip stepped impedance resonator bandpass filter with an extended optimal rejection bandwidth," *IEEE Trans. Microw. Theory Techn.*, vol. 51, no. 5, pp. 1554–1559, May 2003.

[5] G. Chaudhary, Y. Jeong, and J. Lim, "Dual-band bandpass filter with independently tunable center frequencies and bandwidths," *IEEE Trans. Microw. Theory Techn.*, vol. 61, no. 1, pp. 107–116, Jan. 2013.

[6] R. E. Collin, *Foundation for Microwave Engineering*, McGraw-Hill, New York, 1966.

[7] D. Pozar, *Microwave Engineering*, 3rd ed., John Wiley & Sons, New York, 2005.

[8] S. B. Cohn, "Microwave bandpass filters containing high-Q dielectric resonators," *IEEE Trans. Microw. Theory Techn.*, vol. 16, pp. 218–227, Apr. 1968.

[9] K. Zaki and C. Chen, "New results in dielectric-loaded resonators," *IEEE Trans. Microw. Theory Techn.*, vol. MTT-34, no. 7, pp. 815–824, Jul. 1986.

[10] X.-P. Liang and K. Zaki, "Modeling of cylindrical dielectric resonators in rectangular waveguides and cavities," *IEEE Trans. Microw. Theory Techn.*, vol. 41, no. 12, pp. 2174-2181, 1993.

[11] J.-F. Liang and W. D. Blair, "High-Q TE01 mode DR filters for PCS wireless base stations," *IEEE Trans. Microw. Theory Techn.*, vol. 42, no. 12, pp. 2449–2454, Dec. 1994.

[12] R. R. Mansour, "Filter technologies for wireless base stations," *IEEE Microw. Mag.*, vol. 5, pp. 68–74, Mar. 2004.

[13] R. R. Mansour, "Dual-mode dielectric resonator filters with improved spurious performance," *IEEE MTT-S Int. Microw. Symp. Dig.*, 1993.

[14] I. V. Lebedev and E. M. Guttsait, "Resonator of the subcritical waveguide type," *Radiotekh. Elecktron*., pp. 1303-1307, Oct. 1956.

[15] E. T. Jaynes, "Ghost modes in imperfect waveguides," *Proc. IRE*, vol. 46, no. 2, pp. 416–418, Feb. 1958.

[16] W.A. Edson, "Microwave filters using ghost-mode resonance," *Proc. IRE*, vol. 19, pp. 2, 1961.

[17] G. Craven and C. Mok, "The design of evanescent mode waveguide bandpass filters for a prescribed insertion loss characteristic," *IEEE Trans. Microw. Theory Techn.*, vol. MTT-19, no. 3, pp. 295–308, Mar. 1971.

[18] R. V. Snyder, "Dielectric resonator filter with wide stopbands," *IEEE Trans. Microw. Theory Techn.*, vol. 40, pp. 2100–2102, Nov. 1992.

[19] S.-W. Chen, K. A. Zaki, and R. G. West, "Tunable, temperature-compensated dielectric resonators and filters," *IEEE Trans. Microw. Theory Techn.*, vol. 38, no. 8, pp. 1046–1052, Aug. 1990.

[20] R. Zhang and R. R. Mansour, "Dual-band dielectric-resonator filters," *IEEE Trans. Microw. Theory Techn.*, vol. 57, no. 7, pp. 1760–1766, Jul. 2009.

[21] R. J. Cameron, C. M. Kudsia, and R. R. Mansour, *Microwave Filters for Communication Systems: Fundamentals, Design, and Applications*, New York, NY, USA: Wiley, 2007.

[22] A. E. Atia, "Computer-aided design of waveguide multiplexers," *IEEE Trans. Microw. Theory Techn.*, vol. MTT-22, pp. 332–336, Mar. 1974.

[23] C. M. Kudsia, K. R. Ainsworth, and M.V. O'Donovan, "Microwave filters and multiplexing networks for communication satellites in the 1980s," *Proc. AIAA 8th Communications Satellite Systems Conf.*, Apr. 1980.

[24] D. Doust, et al., "Satellite multiplexing using dielectric resonator filters," *Microw. J.*, vol. 32, no. 12, pp. 93-100, Dec. 1989.

[25] D. S. Levinson and R. L. Bennett, "Multiplexing with high performance directional filters," *Microw. J.*, pp. 99–112, June 1989.

[26] C. Kudsia, R. Cameron, and W.-C. Tang, "Innovations in microwave filters and multiplexing networks for communications satellite systems," *IEEE Trans. Microw. Theory Techn.*, vol. 40, no. 6, pp. 1133-1149, June 1992.

[27] S. Ye and R. R. Mansour. "Design of manifold-coupled multiplexers using superconductive lumped element filters." *IEEE MTT-S Int. Microw. Symp. Dig.*, 1994.

[28] R. R. Mansour, S. Ye, V. Dokas, B. Jolley, W.C. Tang, and C. Kudsia, "System integration issues of high power HTS output multiplexers," *IEEE Trans. Microw. Theory Techn.*, vol. MTT-48, pp. 1199–1208, Jul. 2000.

[29] R. J. Cameron, C. M. Kudsia and R. R. Mansour, *Microwave Filters for Communications Systems: Fundamentals, Design, and Applications*, pp. 507-513, 2007.

[30] M. Yu and Y. Wang. "Enhanced microwave multiplexing network," *IEEE Trans. Microw. Theory Techn.*, vol. 59, no. 2, pp. 270-277, Feb. 2007.

[31] J. D. Rhodes and C. I. Mobbs, "Explicit design of remote-tuned combiner for GSM and WCDMA signals," *International Journal of Circuit Theory and Applications*, vol. 35, no. 5-6, pp. 547-564, 2007.

[32] I. C. Hunter, et al., "Transversal directional filters for channel combining," in *IEEE MTT-S Int. Microw. Symp. Dig.*, Seattle, WA, USA, Jun. 2013.

[33] Y. Sun, Y. Wang, M. Yu and J. Liu, "Design of Dual-Band Filter Using Dielectric Resonator and Evanescent Mode Filters," *IEEE International Workshop on Electromagnetics (iWEM2016*), May 16-18, Nanjing, China (accepted).

[34] G. Matthaei, L. Young, and E. M. T. Jones, *Microwave Filters, Impedance-Matching Networks, and Coupling Structures*. Norwood: Artech House, 1964.

[35] T. S. Saad, *Microwave engineers' handbook*, vol. 2. Artech House, 1971.

[36] R. J. Cameron, "General coupling matrix synthesis methods for Chebyshev filtering functions," *IEEE Trans. Microw. Theory Techn.*, vol. 47, no. 4, pp. 433-442, Apr. 1999.

[37] R. J. Cameron, "Advanced coupling matrix synthesis techniques for microwave filters," *IEEE Trans. Microw. Theory Techn.*, vol. 51, no. 1, pp. 1–10, Jan. 2003.

[38] J. W. Bandler and S. H. Chen, "Circuit optimization: the state of the art," *IEEE Trans. Microw. Theory Techn.*, vol. 36, no. 2, pp. 424–443, Feb. 1988.

[39] R. Fletcher, *Practical methods of optimization*. John Wiley & Sons, 2013.

[40] M. B. Steer, J. W. Bandler, and C. M. Snowden, "Computer-aided design of RF and microwave circuits and systems," *IEEE Trans. Microw. Theory Techn.*, vol. 50, no. 3, pp. 996–1005, Mar. 2002.

[41] J. W. Bandler, et al., "Efficient optimization with integrated gradient approximations," *IEEE Trans. Microw. Theory Techn.*, vol. 36, pp. 444-455, Feb. 1988.

[42] R. L. Haupt, "An introduction to genetic algorithms for electromagnetics," *IEEE Antennas and Propagation Mag.*, vol. 37, no. 2, pp. 7-15, 1995.

[43] S. Ye and R. R. Mansour, "An innovative CAD technique for microstrip filter design," *IEEE Microw. Theory Techn.*, vol. 45, no. 5, pp. 780–786, May 1997.

[44] S. F. Peik and R. R. Mansour, "A novel design approach for microwave planar filters," *IEEE MTT-S Int. Microw. Symp. Dig.*, 2002.

[45] S. Bila, et al., "Direct electromagnetic optimization of microwave filters," *IEEE Microw. Mag.*, vol. 2, no. 1, pp. 46–51, Mar. 2001.

[46] J. W. Bandler, R. M. Biernacki, S. H. Chen, P. A. Grobelny, and R. H. Hemmers, "Space mapping technique for electromagnetic optimization," *IEEE Trans. Microw. Theory Techn.*, vol. 42, no. 12, pp. 2536–2544, Dec. 1994.

[47] J. W. Bandler, R. M. Biernacki, S. H. Chen, R. H. Hemmers, and K. Madsen, "Electromagnetic optimization exploiting aggressive space mapping," *IEEE Trans. Microw. Theory Techn.*, vol. 43, no. 12, pp. 2874-2882, Dec. 1995.

[48] J. W. Bandler, R. M. Biemacki, S. H. Chen, and Y. F. Huang, "Design optimization of interdigital filters using aggressive space mapping and decomposition," *IEEE Trans. Microw. Theory Techn.*, vol. 45, pp. 761-769, 1997.

[49] J. W. Bandler, Q. S. Cheng, S. A. Dakroury, A. S. Mohamed, M. H. Bakr, K. Madsen, and J. Søndergaard, "Space mapping: The state of the art," *IEEE Trans. Microw. Theory Techn.*, vol. 52, no. 1, pp. 337–361, Jan. 2004.

[50] M. H. Bakr, J. W. Bandler, K. Madsen, and J. Søndergaard, "Review of the space mapping approach to engineering optimization and modeling," Opt. Eng., vol. 1, pp. 241–276, 2000.

[51] M. A. Ismail, D. Smith, A. Panariello, Y. Wang, and M. Yu, "EM-based design of large-scale dielectric-resonator filters and multiplexers by space mapping," *IEEE Trans. Microw. Theory Techn.*, vol. 52, no. 1, pp. 386–392, Jan. 2004.

[52] Agilent ADS, http://eesof.tm.agilent.com.

[53] Y. Wang and M. Yu, "Inline realization of cascaded trisection and cascaded quadruplet in coaxial cavity filters," Proc. Eur. Microw. Conf., Rome, Italy, 2009, pp. 448–451.

[54] Y. Wang and M. Yu, "True inline cross-coupled coaxial cavity filters, " *IEEE Trans. Microw. Theory Techn.*, vol. 57, no. 12, pp. 2958–2965, Dec. 2009.

[55] J. B. Thomas, "Cross-coupling in coaxial cavity filters—A tutorial overview," *IEEE Trans. Microw. Theory Techn.*, vol. 51, no. 4, pp. 1368–1376, Apr. 2003.

[56] Z. Zakaria, I. C. Hunter, and A. C. Guyette, "Design of coaxial resonator filter with nonuniform dissipation," in *IEEE MTT-S Int. Microw. Symp. Dig.*, 2008, pp. 623–626.

[57] Z. Zakaria, A. Sabah, W. Y. Sam, "Design of low-loss coaxial cavity bandpass filter with post-manufacturing tuning capabilities," *IEEE Symposium on Business, Engineering and Industrial Applications (ISBEIA)*, pp. 733 – 736, 2012.

[58] F.-C. Chen, et al., "Dual-Band Coaxial Cavity Bandpass Filter With Helical Feeding Structure and Mixed Coupling," *IEEE Microwave and Wireless Components Letters*, vol. 25, no. 1, pp. 31-33, 2015.

[59] J. Reed and G. J. Wheeler. "A method of analysis of symmetrical four-port networks," *IEEE Trans. Microw. Theory Techn.*, vol. 4, no.4, pp. 246-252, 1956.

[60] H. Yao, K. A. Zaki, A. E. Atia, and R. Hershtig, "Full wave modeling of conducting posts in rectangular waveguide and its application to slot coupled combline filters, " *IEEE Trans. Microw. Theory Techn.*, vol. 43, pp. 2824–2830, Dec. 1995.

[61] J.–F. Liang, H.–S. Chang, and K. A. Zaki, "Coaxial Probe Modeling in Waveguides and Cavities," *IEEE Trans. Microw. Theory Techn.*, vol. 40, No. 12, pp. 2172–2180, Dec. 1992.

[62] J. R. Reid and R. T. Webster, "A 60 GHz branch line coupler fabricated using integrated rectangular coaxial lines, " in *IEEE MTT-S Int. Microw. Symp. Dig.*, 2004, pp. 441–444.